Journal of Virology®

CELLULAR RESPONSE TO INFECTION

DTX3L Enhances Type I Interferon Antiviral Response by Promoting the Ubiquitination and Phosphorylation of TBK1

Jiaqi Huang,[a] Zhengrong Chen,[a] Yunfei Ye,[b] Yu Shao,[b] Peijie Zhu,[b] Xiaoping Li,[b,c] Yu Ma,[a] Fei Xu,[b] Ji Zhou,[b] Mengyun Wu,[b] Xiu Gao,[b] Yi Yang,[b] Jinping Zhang,[b] Chuangli Hao[a]

[a]Department of Respiratory Medicine, Children's Hospital of Soochow University, Suzhou, People's Republic of China
[b]Institutes of Biology and Medical Sciences, Soochow University, Suzhou, People's Republic of China
[c]Reproductive Medicine Center, the First Affiliated Hospital of Soochow University, Suzhou, People's Republic of China

Jiaqi Huang, Zhengrong Chen, and Yunfei Ye contributed equally to this work. Author order was determined by the time that they first participated in the project.

ABSTRACT Studies already revealed that some E3 ubiquitin ligases participated in the immune response after viral infection by regulating the type I interferon (IFN) pathway. Here, we demonstrated that type I interferon signaling enhanced the translocation of ETS1 to the nucleus and the promoter activity of E3 ubiquitin ligase DTX3L (deltex E3 ubiquitin ligase 3L) after virus infection and thus increased the expression of DTX3L. Further experiments suggested that DTX3L ubiquitinated TBK1 at K30 and K401 sites on K63-linked ubiquitination pathway. DTX3L was also necessary for mediating the phosphorylation of TBK1 through binding with the tyrosine kinase SRC: both together enhanced the activation of TBK1. Therefore, DTX3L, being an important positive-feedback regulator of type I interferon, exerted a key role in antiviral response.

IMPORTANCE Our present study evaluated DTX3L as an antiviral molecule by promoting IFN production and establishing an IFN-β–ETS1–DTX3L–TBK1 positive-feedback loop as a novel immunomodulatory step to enhance interferon signaling and inhibit respiratory syncytial virus (RSV) infection. Our finding enriches and complements the biological function of DTX3L and provides a new strategy to protect against lung diseases such as bronchiolitis and pneumonia that develop with RSV.

KEYWORDS respiratory syncytial virus, type I interferon, deltex E3 ubiquitin ligase 3L, DTX3L, antiviral response

Respiratory syncytial virus (RSV) mainly causes bronchiolitis in infants and is one of the most common causes of hospitalization in infants (1, 2). Currently, the only recommended therapy is supportive since there is no effective vaccine or specific antiviral drug for RSV infection yet (3). Therefore, it is urgent to study the pathogenesis of and to explore the intervention targets for RSV infection.

Type I interferon is the main innate immune barrier for RSV infection (4). RSV RNA could be recognized by retinoic acid-inducible gene I (RIG-I)/melanoma differentiation-associated gene 5 (MDA5) and finally initiates the expression of type I IFN. After IFN is produced, it binds to the coreceptors of IFN-α and IFN-β and activates the ISGF3 complex (IRF9/STAT1/STAT2) through JAK to induce IFN-stimulated gene (ISG) expression (5, 6). But how RSV infection induces the production of IFN is largely unknown.

Type I interferon is produced by several cell types in RSV infection, including dendritic cells (DCs), epithelial cells, fibroblasts, and alveolar macrophages (AMs) (7–10). Studies have shown that AMs are the main source of type I interferon in mice infected with RSV. AMs recognize RSV through RIG-I in the RIG-I-like receptor (RLR) signaling pathway. The interferon produced by AMs locally induces the production of monocyte chemotactic agents

Editor Bryan R. G. Williams, Hudson Institute of Medical Research

Address correspondence to Yi Yang, yangyi87@suda.edu.cn, Jinping Zhang, j_pzhang@suda.edu.cn, or Chuangli Hao, hcl_md@163.com.

The authors declare no conflict of interest.

Received 7 May 2023
Accepted 11 May 2023
Published 31 May 2023

and recruits inflammatory cells in the lung to limit viral load and reduce disease severity (11). Furthermore, macrophages are the main cells infected by RSV (12). Our former study also showed that macrophages are the main cells infected by RSV (data not shown). Thus, macrophages are the key cells of anti-RSV immunity.

E3 ligase is critical for efficient type I IFN production and initiation of antiviral immunity. The levels of expression of RIG-I and interferon are decreased in E3 ubiquitin ligase FBXW7 gene-deficient macrophages (13). TRIM21 promotes CVB3-mediated IRF3 activation and enhances type I interferon signal transduction by interacting with MAVS and catalyzing K27 polyubiquitination of MAVS (14). RNF128 specifically catalyzes the K63 polyubiquitination of TBK1, promoting autophosphorylation of TBK1 and downstream IRF3 activation (15). NRDP1 could promote the activation of TBK1 by modifying the K63 polyubiquitination of TBK1, thus positively regulating the activation of the antiviral innate immune signaling pathway (16). However, few studies have reported which kind of E3 is involved in RSV induced IFN signaling pathway.

In the present study, a mass spectrometry assay showed that deltex E3 ubiquitin ligase 3L (DTX3L [also known as BBAP]) was obviously increased in RSV-infected RAW264.7 cells compared to noninfected cells. Extensive studies showed that type I interferon receptor signaling promoted ETS1 to become involved in the nuclear and the promoter activity of DTX3L in RSV infection and thus increased the expression of DTX3L. Further experiments suggested that DTX3L ubiquitinated TBK1 at K30 and K401 sites on the K63-linked ubiquitination pathway. On the other hand, DTX3L was also necessary for mediating the phosphorylation of TBK1 through binding with SRC: both together enhanced the activation of TBK1. So DTX3L is an important positive-feedback regulator of type I interferon in RSV infection.

RESULTS

RSV infection induces DTX3L expression in macrophages. RSV type L19 tagged with mCherry (RSV-mCherry) was used to stimulate RAW264.7 cells. After RSV infection, RAW264.7 cells showed increasing red fluorescence (Fig. 1A and B) and RSV mRNA expression (Fig. 1C and D), which indicated that RSV had successfully infected the RAW264.7 cells. To screen which kind of E3 ligase is involved in RSV-infected RAW264.7 cells, mass spectrometry was conducted to detect the expression of different proteins after RSV infection. Thirty-one E3 ubiquitin ligase and deubiquitin enzymes were differently expressed among RSV-infected and nontreated RAW264.7 cells (Fig. 1E). The reliability of the mass spectrometry results was confirmed by using real-time quantitative PCR (qPCR) to detect some selected molecules (data not shown); the result was consistent with the mass spectrometry experiment. E3 ubiquitin ligase DTX3L showed increasing expression in RAW264.7 cells after RSV infection (Fig. 1F and G) and also in other RNA virus-infected and poly(I·C)-stimulated RAW264.7 cells (Fig. 1H to K). In addition, DTX3L expression was increased in bone marrow derived-macrophages (BMDMs) (Fig. 1L) after RSV infection. These results demonstrated that DTX3L was closely related to virus infection.

Interestingly, a previous study reported that the expression of DTX3L and PARP9 was increased in response to IFN-β in U3A cell lines (17). Consistent with their results, we found the expression of DTX3L was increased in IFN-β-stimulated RAW264.7 cells (Fig. 1M and N). To our surprise, the expression of DTX3L in peritoneal macrophages of type I IFN receptor knockout (KO) (IFNAR1$^{-/-}$) mice was not increased after RSV infection compared to that in wild-type (WT) mouse peritoneal macrophages infected with RSV (Fig. 1O). These results indicated that the increasing expression of DTX3L stimulated by RSV depended on the interaction between type I interferon and type I interferon receptor.

Type I IFN enhances the translocation of ETS1 to the nucleus and DTX3L promoter activation. Since DTX3L increased in virus-stimulated macrophages, we explored how DTX3L expression increased by RSV. We hypothesize that there may be some transcription factors induced by RSV that therefore activate the DTX3L promoter and its expression. The analysis according to scores in programs in JASPAR

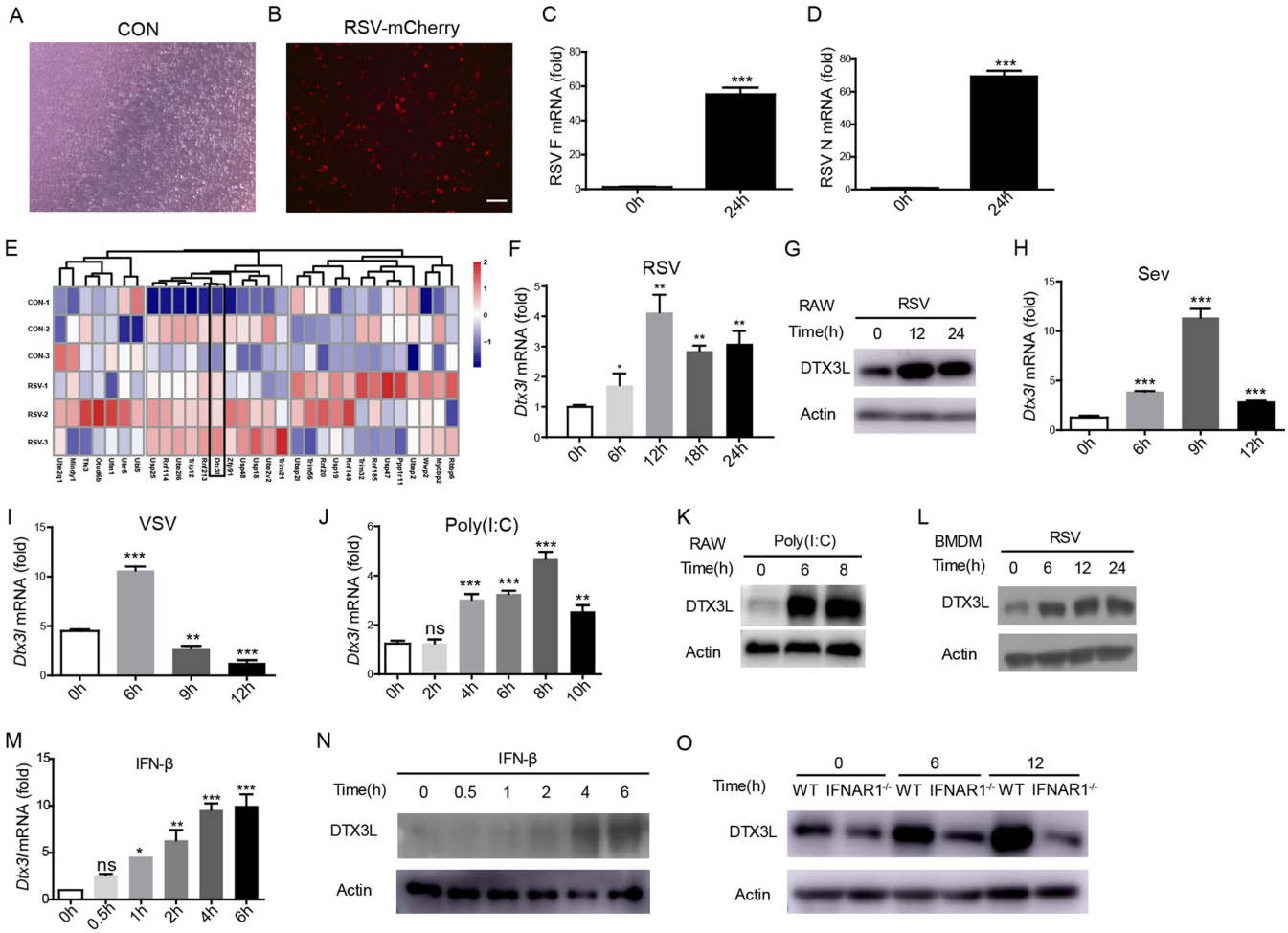

FIG 1 DTX3L is induced by RSV infection or IFN-β stimulation. (A and B) mCherry fluorescence ($\times$200 magnifications) and (C and D) RSV F and N mRNA expression were detected in RSV-infected RAW264.7 cells (MOI of 10) at 24 h postinfection (hpi). CON, control. Scale bars, 100 μm. (E) Heat map of protein profiles in RAW264.7 cells infected with RSV (MOI of 10) at 24 hpi; (F) *Dtx3l* mRNA expression in RAW264.7 cells infected with RSV (MOI of 10) for 0, 6, 12, 18, and 24 h; (G) immunoblot analysis of DTX3L expression in RAW264.7 cells upon infection with RSV (MOI of 10) for 0, 12, and 24 h; (H to J) qPCR analysis of *Dtx3l* mRNA expression in RAW264.7 cells upon infection with SeV (MOI of 1) (H) and VSV (MOI of 1) (I) for 0, 6, 9, and 12 h or stimulation with poly(I·C) (10 μg/mL) (J) for 0, 2, 4, 6, 8, and 10 h; (K) immunoblot analysis of DTX3L expression in RAW264.7 cells upon stimulation with poly(I·C) (10 μg/mL) for 0, 6, and 8 h; (L) immunoblot analysis of DTX3L expression in BMDMs upon infection with RSV (MOI of 10) for 0, 6, 12, and 24 h; (M and N) *Dtx3l* mRNA (M) and DTX3L protein (N) expression in RAW264.7 cells stimulated with IFN-β (3,000 U/mL) for 0, 0.5, 1, 2, 4, and 6 h; (O) immunoblot analysis of DTX3L in peritoneal macrophages of WT and IFNAR1$^{-/-}$ mice infected with RSV (MOI of 10). All qPCR results are represented as relative fold changes after normalization to *Gapdh* controls. Results are expressed as mean $\pm$ SEM and are representative of at least three independent experiments. ns, not significant ($P > 0.05$); *, $P < 0.05$; **, $P < 0.01$; ***, $P < 0.001$.

(http://jaspar.genereg.net/analysis) indicated that transcription factor ETS1 might be bound to the promoter of *Dtx3l*. The endogenous ETS1 was associated with the DTX3L promoter at NC_000082.6 (35939027 to 35941027), and the predicted sequence is CTTCCG. ETS1 transcription factor regulates numerous genes and is involved in stem cell development, cell aging and death, and tumorigenesis (18). To investigate whether ETS1 regulates *Dtx3l* promoter and its expression, HEK293T cells were cotransfected with pcDNA3.1-ETS1 (full-length encoded plasmid of transcription factor ETS1) and pGL3-DTX3L (DTX3L promoter luciferase reporter plasmid), *Dtx3l* promoter activity was measured using a dual-luciferase reporter system. We found that the promoter activity of DTX3L could be significantly enhanced by ETS1 (Fig. 2A).

Previous data showed that RSV could upregulate DTX3L expression by promoting type I IFN production; therefore, we speculated whether there was some kind of relationship between RSV and transcription factor ETS1. The difference in expression levels of ETS1 between RSV-infected and control RAW264.7 cells was measured by qPCR.

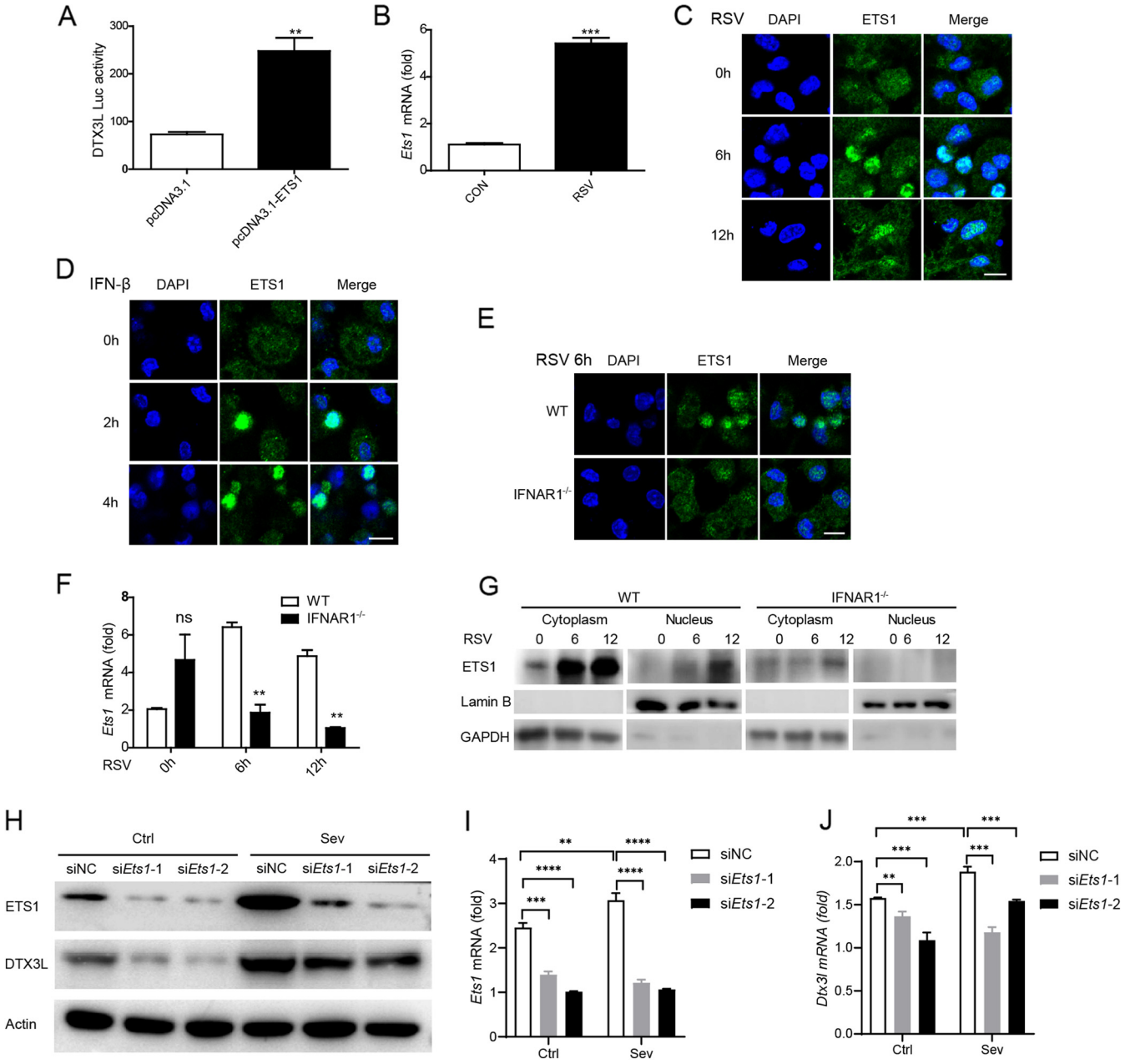

FIG 2 RSV enhances translocation of ETS1 to the nucleus and its activation of DTX3L promoter. (A) HEK293T cells were cotransfected with a *Dtx3l* promoter luciferase reporter plasmid (pGL3-DTX3L-Promoter) and full-length encoded plasmid for transcription factor ETS1 (pcDNA3.1-ETS1). The relative activity of *Dtx3l* promoter was measured using a luciferase reporter system. (B) *Ets1* mRNA expression in RAW264.7 cells infected with RSV (MOI of 10) at 6 hpi. CON, control. (C and D) Peritoneal macrophages of WT mice were infected with RSV (MOI of 10) for 0, 6, and 12 h (C) or stimulated with IFN-β (3,000 U/mL) for 0, 2, and 4 h (D). Endogenous ETS1 protein and nucleus were stained with anti-ETS1 antibody (green) and DAPI dye (blue) and observed under a confocal microscope. Photomicrographs were captured under high-power fields ($\times$600 magnifications). Scale bars, 10 μm. (E) Peritoneal macrophages of WT and IFNAR1$^{-/-}$ mice were infected with RSV (MOI of 10) for 6 h. Endogenous ETS1 protein and nucleus were stained with anti-ETS1 antibody (green) and DAPI dye (blue) and observed under a confocal microscope. Photomicrographs were captured under high-power fields ($\times$600 magnifications). Scale bars, 10 μm. (F) qPCR analysis of *Ets1* mRNA in WT and IFNAR1$^{-/-}$ peritoneal macrophages infected with RSV (MOI,10) for 0, 6, and 12 h; (G) immunoblot analysis of ETS1 among nuclear and cytoplasm proteins from peritoneal macrophages of WT and IFNAR1$^{-/-}$ mice stimulated with RSV (MOI of 10). Lamin B serves as a nuclear control, and GAPDH serves as a cytoplasm control. (H) Control- or *Ets1* siRNA-transfected NIH 3T3 cells were infected with SeV (MOI of 1) for 6 h, and the cell lysates were collected for immunoblotting. (I and J) Control- or *Ets1* siRNA-transfected NIH 3T3 cells were infected with SeV (MOI of 1) for 6 h, and the levels of mRNA expression of Ets1 (I) and DTX3L (J) were measurement by qPCR. All qPCR results are represented as relative fold changes after normalization to *Gapdh* controls (normalized controls [NC]). Results are expressed as mean $\pm$ SEM and are representative of at least three independent experiments. ns, not significant ($P > 0.05$); ***, $P < 0.001$.

Expression of ETS1 was significantly higher in RSV-infected RAW264.7 cells (Fig. 2B). Moreover, translocation of ETS1 to the nucleus increased in peritoneal macrophages of WT mice after RSV infection and IFN-β stimulation (Fig. 2C and D). However, there was no translocation of ETS1 in IFNAR1$^{-/-}$ peritoneal macrophages infected with RSV (Fig.

2E). In addition, *Ets1* mRNA expression was decreased in IFNAR1$^{-/-}$ peritoneal macrophages compared with WT peritoneal macrophages after RSV infection (Fig. 2F). Western blotting results showed that the expression of ETS1 was increased in the nucleus of peritoneal macrophages of WT mice infected with RSV compared to noninfected RSV peritoneal macrophages; this phenomenon was attenuated in the nucleus of peritoneal macrophages of IFNAR1$^{-/-}$ mice (Fig. 2G). To investigate whether ETS1 is needed for DTX3L induction, we transfected NIH 3T3 cells with *Ets1* small interfering RNA (siRNA) and examined its effects on DTX3L induction. The expression of DTX3L were attenuated in NIH 3T3 cells treated with *Ets1* siRNA following virus infection (Fig. 2H to J). These results suggested that transcription factor ETS1 could be upregulated by type I IFN with RSV infection, which consequently contributed to the expression of DTX3L.

DTX3L suppresses RSV replication and promotes type I interferon production. To test the possible role of DTX3L in RSV infection, three specific short hairpin RNAs (shRNAs) targeting the coding sequences of DTX3L were designed and transfected to RAW264.7 cells. shRNA1, which led to large reductions in the overall levels of the DTX3L protein, was used for further study (Fig. 3A). RAW264.7 cells were stably transduced with lentivirus encoding pLL3.7 vector or shRNA specific for DTX3L and then infected with RSV-mCherry (Fig. 3B). DTX3L-downregulated RAW264.7 cells showed increased RSV F mRNA expression (Fig. 3C) and mCherry-positive cells (Fig. 3D) when infected with RSV-mCherry. Furthermore, when BMDMs of WT and *Dtx3l* knockout (*Dtx3l*$^{-/-}$) mice and TC1 cells were infected with RSV, the RSV titer and RSV F mRNA expression were also increased in *Dtx3l*$^{-/-}$ BMDMs (Fig. 3E and F) and DTX3L-downregulated TC1 cells (data not shown). These results strongly suggested that DTX3L significantly restricted RSV replication.

Type I interferons (IFNs) play an important role in the resistance to viral infection. Levels of production of *Ifna* and *Ifnb* mRNA in DTX3L-deficient RAW264.7 cells upon RSV infection were examined by qPCR. In comparison to vector-transfected cells, an obvious decrease in *Ifn* mRNA levels was observed in the DTX3L-deficient cells (Fig. 3G and H). *Ifn* mRNA levels was decreased in BMDMs of *Dtx3l*$^{-/-}$ mice compared with those of WT mice (Fig. 3I and J).

To further verify the function of DTX3L on IFN production, a dual-luciferase reporter assay of IFN-β activity was conducted in B16 cells cotransfected with IFN-β–luciferase reporter plasmid and DTX3L full-length encoded plasmid or control vector. We found that, after stimulation with RIG-IN or RSV, the IFN-β activity was increased when DTX3L was overexpressed: this indicated that DTX3L could promote the generation of IFN-β (Fig. 3K).

Next, interferon-stimulated gene (ISG) mRNA expression was detected, and ISGs such as *Oas1*, *Isg15*, and *Ifit1* also showed an obvious decrease in DTX3L-deficient cells stimulated with RSV (Fig. 3L to N). *Oas1* and *Isg15* were also decreased in BMDMs of *Dtx3l*$^{-/-}$ mice (Fig. 3O and P), while there was no significant change of *Ifit1* mRNA expression (data not shown). These results presented above indicated that DTX3L promotes the interferon antiviral response.

To explore whether viral nucleic acids or viral proteins was involved in the antiviral effect of DTX3L, poly(I·C), a "mimic" of double-stranded viral RNA, was used to stimulate the RAW264.7 cells. We observed the same results as with viral stimulation. We found impaired *Ifnb* and *Oas1*, *Isg15*, and *Ifit1* mRNA levels in DTX3L-deficient cells (Fig. 4A to D). However, inhibition of DTX3L expression did not impact mRNA levels of other proinflammatory cytokines such as *Il6*, *Cxcl2*, and *Tnf*α in RAW264.7 cells (Fig. 4E to G) and *Il6*, *Cxcl1*, and *Tnf*α in BMDMs (Fig. 4H to J). These results indicated that DTX3L promotes the interferon response after viral nucleic acid stimulation.

To verify that DTX3L suppressed RSV replication through IFN generation, we treated WT and *Dtx3l*$^{-/-}$ BMDMs with blocking antibody against IFNAR1 to rule out any other DTX3L-regulated pathways in the observed viral phenotype, with purified mouse IgG1 antibody functioning as irrelevant, isotype-matched control antibody. The results

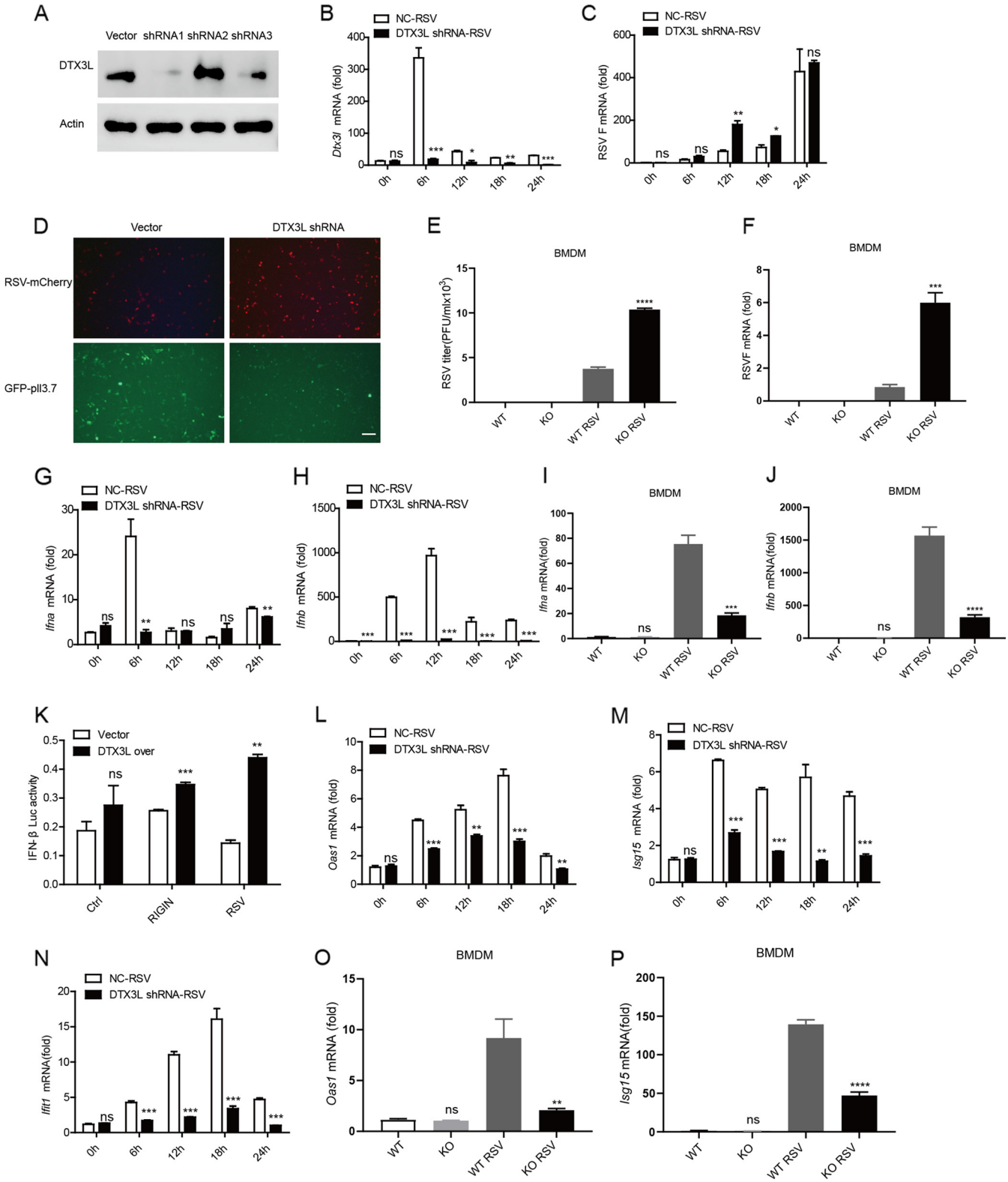

FIG 3 DTX3L suppresses RSV replication and positively regulates type I interferon production. (A) RAW264.7 cells were transfected with pLL3.7 vector or DTX3L shRNAs. Forty-eight hours later, cells were collected and subjected to immunoblot analysis of DTX3L expression. shRNA1 was used for the subsequent experiments. (B) qPCR analysis of *Dtx3l* mRNA expression in RAW264.7 cells stably transduced with lentivirus encoding pLL3.7 vector or shRNA specific for DTX3L, followed by RSV infection (MOI of 10) for 0, 6, 12, 18, and 24 h; (C) expression of RNA encoding RSV fusion protein (RSV F) in RAW264.7 cells stably transduced with lentivirus encoding pLL3.7 vector or shRNA specific for DTX3L, followed by RSV infection (MOI of 10) for 0, 6, 12, 18, and 24 h; (D) mCherry fluorescence (×200 magnifications) detection of RAW264.7 cells stably transduced with lentivirus encoding pLL3.7 vector or shRNA specific for DTX3L, followed by RSV infection (MOI of 10) for 24 h. Scale bars, 100 μm. (E) Plaque assay of RSV titer of the culture supernatants in WT and *Dtx3l*$^{-/-}$

(Continued on next page)

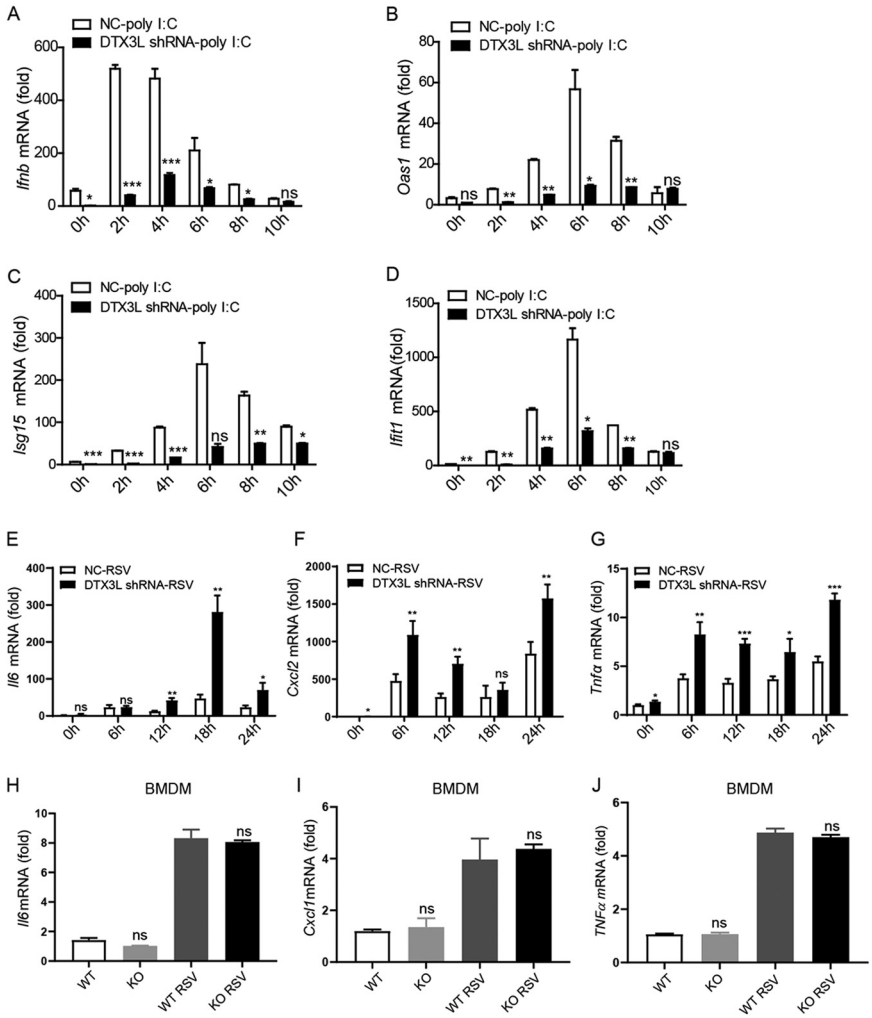

FIG 4 DTX3L positively regulates IFN-β signaling. (A) qPCR analysis of *Ifnb* mRNA in RAW264.7 cells stably transduced with lentivirus encoding pLL3.7 vector or shRNA specific for DTX3L, followed by poly(I·C) stimulation for 0, 2, 4, 6, 8, and 10 h; (B to D) qPCR analysis of *Oas1* (B), *Isg15* (C), and *Ifit1* (D) mRNA in RAW264.7 cells stably transduced with lentivirus encoding pLL3.7 vector or shRNA specific for DTX3L, followed by poly(I·C) stimulation for 0, 2, 4, 6, 8, and 10 h; (E to G) qPCR analysis of *Il6* (E), *Cxcl2* (F), and *Tnfα* (G) mRNA in RAW264.7 cells stably transduced with lentivirus encoding pLL3.7 vector or shRNA specific for DTX3L infected with RSV (MOI of 10); (H to J) qPCR analysis of *Il6* (H), *Cxcl1* (I), and *Tnfα* (J) mRNA in WT and *Dtx3l*$^{-/-}$ bone marrow-derived macrophage (BMDMs) infected with RSV (MOI of 10) for 12 h. All qPCR results are represented as relative fold changes after normalization to *Gapdh* controls. Results are expressed as mean ± SEM and are representative of at least three independent experiments. ns, not significant ($P > 0.05$); **, $P < 0.01$; ***, $P < 0.001$.

showed that knockout of DTX3L promoted RSV infection (Fig. 5A and B), while inhibiting *Ifna*, *Ifnb*, *Oas1*, *Isg15*, and *Ifit1* mRNA expression in BMDMs in the presence of IFNAR1 (Fig. 5C to G). However, knockout of DTX3L did not noticeably affect viral infection (Fig. 5A and B) and *Oas1*, *Isg15*, and *Ifit1* mRNA expression (Fig. 5E to G) in IFNAR1-

FIG 3 Legend (Continued)
bone marrow-derived macrophage (BMDMs) infected with RSV (MOI of 10) for 12 h; (F) expression of RNA encoding RSV fusion protein (RSV F) in WT and *Dtx3l*$^{-/-}$ BMDMs treated as in panel E; (G and H) qPCR analysis of *Ifna* (G) and *Ifnb* (H) mRNA in RAW264.7 cells stably transduced with lentivirus encoding pLL3.7 vector or shRNA specific for DTX3L, followed by RSV infection (MOI of 10) for 0, 6, 12, 18, and 24 h; (I and J) qPCR analysis of *Ifna* (I) and *Ifnb* (J) mRNA in WT and *Dtx3l*$^{-/-}$ BMDMs infected with RSV (MOI of 10) for 12 h. (K) B16 cells were cotransfected with the *Ifnb* promoter reporter plasmids and DTX3L full-length encoded plasmid or control vector and RIG-IN expression plasmid. Forty-eight hours later, cells were infected with RSV (MOI of 1) for 12 h, and the luciferase activity was determined. (L to N) qPCR analysis of *Oas1* (L), *Isg15* (M), and *Ifit1* (N) mRNA in RAW264.7 cells stably transduced with lentivirus encoding pLL3.7 vector or shRNA specific for DTX3L, followed by RSV infection (MOI of 10) for 0, 6, 12, 18, and 24 h. (O and P) qPCR analysis of *Oas1* (O) and *Isg15* (P) mRNA in WT and *Dtx3l*$^{-/-}$ BMDMs infected with RSV (MOI of 10) for 12 h. All qPCR results are represented as relative fold changes after normalization to *Gapdh* controls. Results are expressed as mean ± SEM and are representative of at least three independent experiments. ns, not significant ($P > 0.05$); *, $P < 0.05$; **, $P < 0.01$; ***, $P < 0.001$.

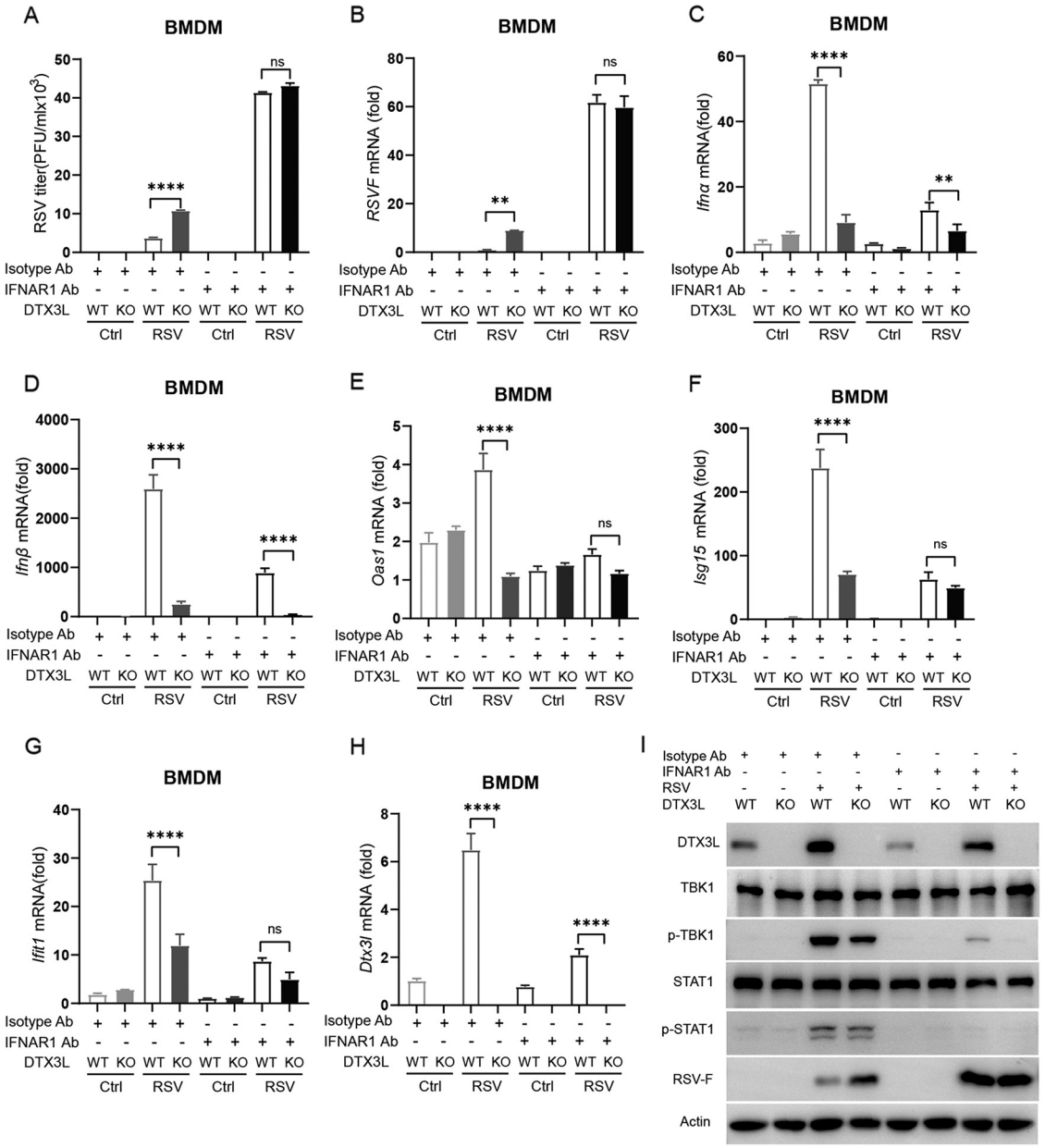

FIG 5 DTX3L promotes virus-induced production of type I IFNs. (A) Plaque assay of RSV titer of the culture supernatants in WT and *Dtx3l*$^{-/-}$ bone marrow-derived macrophage (BMDMs) treated with anti-IFNAR1 blocking antibody (500 ng/mL) and purified mouse IgG1 antibody (500 ng/mL) functioning as an irrelevant, isotype-matched control antibody and then infected with RSV (MOI of 10) for 12 h; (B) qPCR analysis of RNA encoding RSV fusion protein (RSV F) in WT and *Dtx3l*$^{-/-}$ BMDMs treated as in panel A; (C and D) qPCR analysis of *Ifna* (C) and *Ifnb* (D) mRNA in WT and *Dtx3l*$^{-/-}$ BMDMs treated as in panel A; (E to G) qPCR analysis of *Oas1* (E), *Isg15* (F), and *Ifit1* (G) mRNA in WT and *Dtx3l*$^{-/-}$ BMDMs treated as in panel A; (H) qPCR analysis of *Dtx3l* mRNA expression in WT and *Dtx3l*$^{-/-}$ BMDMs treated as in panel A; (I) immunoblot analysis of DTX3L, TBK1, p-TBK1, STAT1, p-STAT1, and RSV fusion protein (RSV F) in WT and *Dtx3l*$^{-/-}$ BMDMs treated with anti-IFNAR1 blocking antibody (500 ng/mL) and purified mouse IgG1 antibody (500 ng/mL) functioning as an irrelevant, isotype-matched control antibody and then infected with RSV (MOI of 10) for 24 h.

blocking BMDMs, while still decreasing *Ifna* and *Ifnb* expression (Fig. 5C and D) and TBK1 phosphorylation (Fig. 5I). These findings suggested that DTX3L-mediated antiviral activity was mediated via type I IFN and provided further evidence that DTX3L could promote the expression of type I IFN upstream of IFNAR1.

TBK1 interacts with DTX3L. Since DTX3L promotes IFN-β production after RSV infection, we suggest that DTX3L might positively modulate the molecules of the type I interferon signaling pathway. To investigate the effect of DTX3L on interferon-related

proteins, RAW264.7 cells stably transduced with lentivirus encoding pLL3.7 vector or shRNA specific for DTX3L and BMDMs prepared from WT and *Dtx3l*$^{-/-}$ mice were infected with RSV. Results showed that the phosphorylation of TBK1 was significantly inhibited in BMDMs of *Dtx3l*$^{-/-}$ mice infected with RSV (Fig. 6A) or Sendai virus (SeV) (Fig. 6B), and DTX3L downregulated RAW264.7 cells infected with RSV (Fig. 6C). In contrast, RIG-I, MAVS, p65, p38, and phosphorylation of p65 and p38 mitogen-activated protein kinase (MAPK) were not impaired in DTX3L-downregulated RAW264.7 cells after infection (Fig. 6D). In addition, we found TBK1 phosphorylation was decreased in DTX3L-downregulated RAW264.7 cells with RSV (Fig. 6E) and SeV (Fig. 6F) infection at different infection times. In addition, a native PAGE assay was performed and demonstrated that downregulation of DTX3L decreased the dimerization of IRF3 (Fig. 6F). These data suggested that DTX3L might enhance type I interferon signaling by targeting TBK1 and was not RSV specific.

An *in vitro* experiment indicated that DTX3L interacted with TBK1 in 293T cells cotransfected with DTX3L and TBK1 full-length encoded plasmids (Fig. 6G). Immunofluorescence assay was conducted to further verify the relationship between DTX3L and TBK1, we found that DTX3L had a more colocalization with TBK1 during the response to RSV infection (Fig. 6H). Furthermore, coimmunoprecipitation and immunoblotting were used to confirm the interaction between DTX3L and TBK1. Endogenous DTX3L and TBK1 coimmunoprecipitated in RAW264.7 cells and BMDMs with RSV (Fig. 6I and K) and poly(I·C) stimulation (Fig. 6J and L), suggesting a constitutive interaction between the two proteins. Notably, the interaction between endogenous DTX3L and TBK1 was enhanced upon RSV infection and poly(I·C) stimulation (Fig. 6I to L). Overall, these results demonstrated that DTX3L targeted and interacted with TBK1.

DTX3L positively regulates K63-linked ubiquitination of TBK1. Since TBK1 was not decreased in DTX3L-deficient RAW264.7 cells, this may implicate DTX3L in playing a role in signal transduction instead of degrading TBK1 by ubiquitination. To investigate whether the E3 ligase activity of DTX3L was involved in the regulation of TBK1 activation, endogenous immunoprecipitation was conducted in BMDMs (Fig. 7A) and RAW264.7 cells (Fig. 7B). The level of ubiquitination of TBK1 was decreased in DTX3L-deficient macrophages, which indicated that DTX3L could increase the ubiquitination of TBK1 (Fig. 7A and B). Moreover, HEK293T cells were cotransfected with full-length encoded plasmids of Myc-TBK1, Flag-DTX3L, and hemagglutinin (HA)-ubiquitin mutants in which all lysine residues except K27, K48, or K63 were replaced with arginine. DTX3L-mediated polyubiquitination of TBK1 was significantly increased in the presence of HA-ubiquitin-tagged K63 but not HA-ubiquitin-K48 and -K27 (Fig. 7C). Taken together, these data demonstrated that DTX3L interacted with TBK1 and promoted K63-linked ubiquitination of TBK1.

It has been reported that K63-linked polyubiquitination of TBK1 at K30 and K401 is required for its activation (15, 19). To investigate whether DTX3L promotes TBK1 ubiquitination through K30 or K401, Myc-TBK1 variant plasmids with point mutations K30R and K401R and two other prediction sites, K137R and K154R, were constructed and transfected into HEK293 cells together with DTX3L full-length encoded plasmid. Myc-TBK1-K30R and Myc-TBK1-K401R, but not Myc-TBK1-K137R and Myc-TBK1-K154R, showed low TBK1 ubiquitination induced by DTX3L (Fig. 7D). These data demonstrated that DTX3L promoted K63-linked ubiquitination of TBK1 at K30 and K401.

DTX3L promotes phosphorylation of TBK1 through SRC. Activation of TBK1 also needs its autophosphorylation (20); how DTX3L promotes the phosphorylation of TBK1 remains unclear. To our knowledge, there were several kinases upstream of TBK1 that might regulate its phosphorylation and kinase activity. Glycogen synthase kinase 3β (GSK-3β) is implicated in promoting the autophosphorylation of TBK1 (21). The tyrosine kinase SRC promotes phosphorylation of the kinase TBK1 to facilitate type I interferon production after viral infection (22). Furthermore, TBK1 could interact with the adaptor proteins TANK (TRAF family member associated NF-κB activator) and NEMO (NF-κB essential modulator), which are required for its activation (23). On the basis of these results, we hypothesize that DTX3L may regulate the binding strength between these adapters and p-TBK1. To verify this hypothesis, the interaction between p-TBK1 and these kinases was

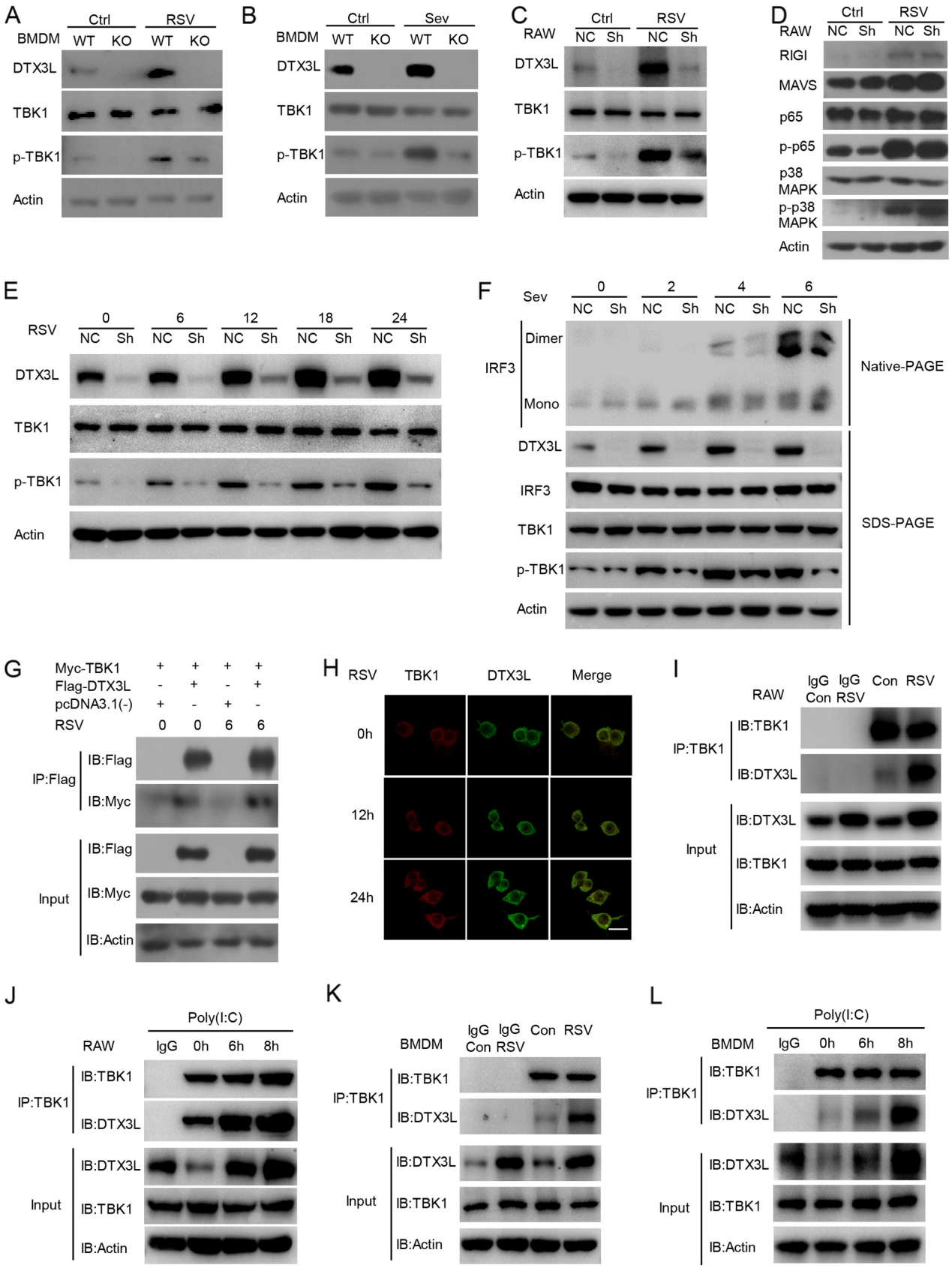

FIG 6 DTX3L promotes phosphorylation of TBK1 and interacts with TBK1. (A and B) Immunoblot analysis of DTX3L, TBK1, and p-TBK1 in WT and *Dtx3l*$^{-/-}$ BMDMs infected with RSV (MOI of 10) for 24 h (A) and SeV (MOI of 1) for 6 h (B). Actin served as the control. Ctrl, control (no infection).

(Continued on next page)

detected in both BMDMs and RAW264.7 cells. The results showed that TBK1 phosphorylation was lower in BMDMs of *Dtx3l*$^{-/-}$ mice (Fig. 8A) and DTX3L downregulated RAW264.7 cells after RSV infection (Fig. 8B). In addition, we found DTX3L could interact with SRC, and this binding decreased when inhibited DTX3L expression (Fig. 8A and B), but we did not observe the similar results in NEMO, GSK-3β and TANK immunoprecipitation experiments with BMDMs (Fig. 8A) and RAW264.7 cells (Fig. 8B). A similar phenomenon was observed in poly(I·C)-stimulated RAW264.7 cells (Fig. 8C). We then treated HEK293T cells with Src siRNA and examined its effects on DTX3L-TBK1 interaction. The interactions of endogenous DTX3L and TBK1 were attenuated in 293T cells treated with Src siRNA (Fig. 8D). All of the above results together suggested that DTX3L regulated the phosphorylation of TBK1 through binding with SRC.

Ablation of DTX3L renders mice susceptible to RNA virus infection. To further confirm the antiviral effect of DTX3L *in vivo*, *Dtx3l*$^{-/-}$ mice was constructed by a CRISPR/Cas9 strategy as described in Materials and Methods (Fig. 9A). Genotyping and Western blot results demonstrated that the *Dtx3l*$^{-/-}$ mouse model was successfully established (Fig. 9B and C). WT and *Dtx3l*$^{-/-}$ mice were infected intranasally with RSV. *Dtx3l*$^{-/-}$ mice exhibited significantly increased lymphocyte infiltration and alveolar inflammatory exudation compared with WT mice (Fig. 10A and B). The plaque assay and real-time PCR results indicated that RSV infection was increased in *Dtx3l*$^{-/-}$ mice (Fig. 10C and D). These data confirmed that DTX3L effectively suppressed RSV replication *in vivo*. Then we performed flow cytometry analyses to determine the cellular infiltrate differences in the absence of DTX3L. The percentages of F4/80^{+} CD11b^{+} macrophages were higher in the peripheral blood mononuclear cells (PBMCs) of *Dtx3l*$^{-/-}$ mice (Fig. 10E and F) than in those of the WT mice, indicating an accumulation of macrophages and more inflammation in the *Dtx3l*$^{-/-}$ mice. CD11b^{+} Ly6G^{+} neutrophils were slightly higher in the PBMCs of *Dtx3l*$^{-/-}$ mice, with no significant difference (data not shown). There were no significant differences in B/T lymphocytes (data not shown). Furthermore, WT and *Dtx3l*$^{-/-}$ mice were infected intranasally with vesicular stomatitis virus (VSV) for 24 h. Deletion of DTX3L resulted in increased VSV loads and decreased type I IFN response *in vivo*, as evidenced by increased VSV titer (Fig. 10G) and VSV RNA level (Fig. 10H) and decreased TBK1, IRF3, and STAT1 phosphorylation (Fig. 10I) and *Ifn*β and *Isgs* mRNA levels in mouse lung (Fig. 10J to M). Taken together, these findings suggest that DTX3L regulates type I IFN-mediated signaling and antiviral activity *in vivo*.

Our present study first demonstrates that DTX3L is a positive-feedback regulator of type I IFN and is involved in anti-RSV response *in vivo* and *in vitro*. Mechanically, we identified RSV and IFN-β could enhance the translocation of ETS1 to the nucleus to promote the expression of DTX3L. DTX3L as an E3 ligase ubiquitinates TBK1 at K30 and K401 in the K63-linked polyubiquitination pathway and promotes the phosphorylation of TBK1 through binding with SRC, enhancing the type I interferon antiviral response (Fig. 11).

FIG 6 Legend (Continued)
(C) Immunoblot analysis of DTX3L, TBK1, and p-TBK1 in RAW264.7 cells stably transduced with lentivirus encoding pLL3.7 vector or shRNA specific for DTX3L, followed by RSV infection (MOI of 10) for 24 h. Actin served as the control. (D) Immunoblot analysis of RIGI, MAVS, p65, phosphorylated p65 (p-p65), p-38 MAPK, and p-p38 in RAW264.7 cells stably transduced with lentivirus encoding pLL3.7 vector or shRNA specific for DTX3L, followed by RSV infection (MOI of 10) for 24 h. Actin served as the control. (E) Immunoblot analysis of DTX3L, TBK1, and p-TBK1 in RAW264.7 cells stably transduced with lentivirus encoding pLL3.7 vector or shRNA specific for DTX3L, followed by RSV infection (MOI of 10) for 0, 6, 12, 18, and 24 h. Actin served as the control. (F) Immunoblot analysis of DTX3L, TBK1, and p-TBK1 and native PAGE for the detection of IRF3 dimerization in RAW264.7 cells stably transduced with lentivirus encoding pLL3.7 vector or shRNA specific for DTX3L, followed by Sev infection (MOI of 1) for 0, 2, 4, and 6 h. Actin served as the control. (G) HEK293T cells were cotransfected with Myc-TBK1 and Flag-DTX3L full-length encoded plasmids and pcDNA3.1(−) plasmids. Forty-eight hours later, cells were infected with RSV (MOI of 1) for 6 h. Cellular lysates were immunoprecipitated with anti-Flag. Immunoprecipitates were analyzed by immunoblotting with anti-Flag and anti-Myc. (H) RAW264.7 cells were infected by RSV (MOI of 10) for 0, 12, and 24 h. Endogenous DTX3L, TBK1 protein, and nucleus stained with anti-DTX3L antibody (green) and anti-TBK1 antibody (red) and observed under a confocal microscope. Photomicrographs were captured under high-power fields (×600 magnifications). Scale bars, 10 μm. (I) Immunoprecipitation and immunoblot analysis of DTX3L and TBK1 in RAW264.7 cells infected with RSV (MOI of 10) for 12 h; (J) immunoprecipitation and immunoblot analysis of DTX3L and TBK1 in RAW264.7 cells stimulated with poly(I·C) for 0, 6, and 8 h; (K) immunoprecipitation and immunoblot analysis of DTX3L and TBK1 in BMDMs infected with RSV (MOI of 10) for 12 h; (L) immunoprecipitation and immunoblot analysis of DTX3L and TBK1 in BMDMs cells stimulated with poly(I·C) for 0, 6, and 8 h. Results are representative of at least three independent experiments.

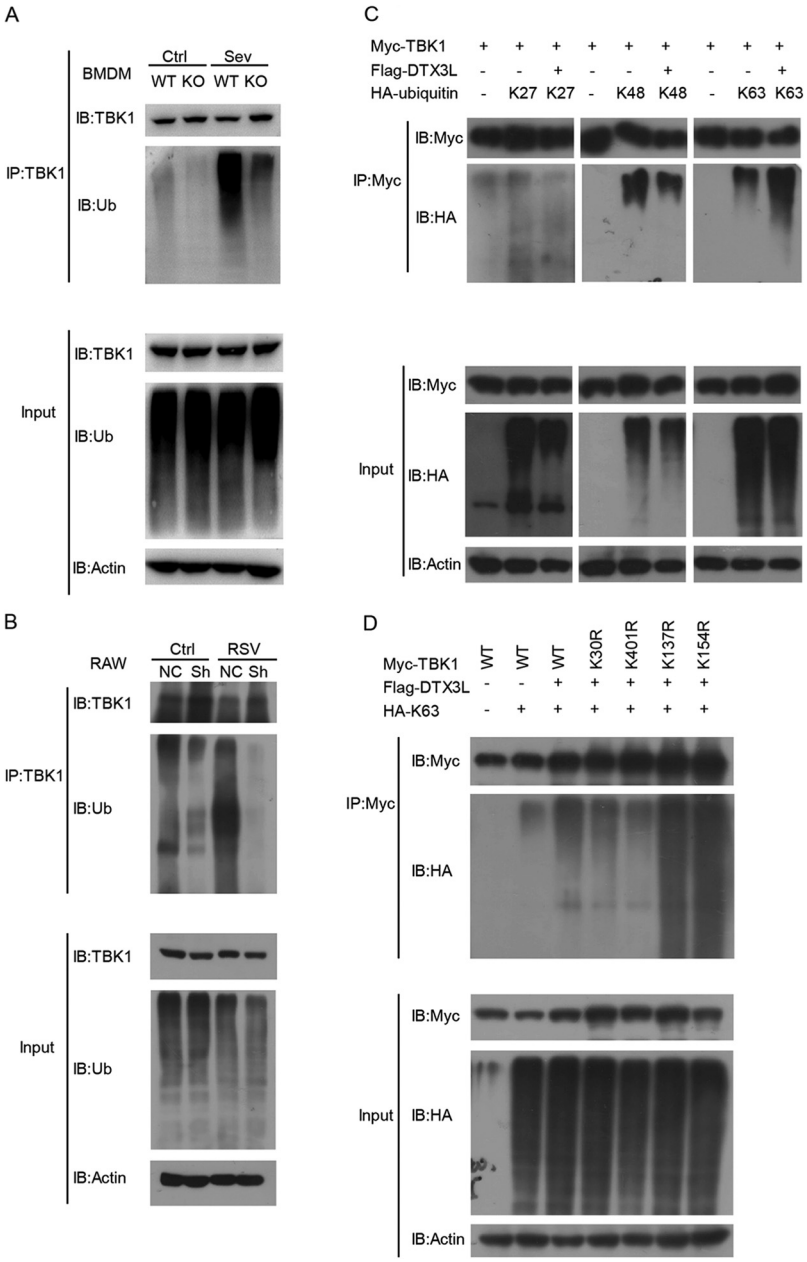

FIG 7 DTX3L positively regulates K63-linked ubiquitination of TBK1. (A and B) Immunoprecipitation and immunoblot analysis of endogenous TBK1 and ubiquitin in WT and *Dtx3l*$^{-/-}$ BMDMs infected with SeV (MOI of 1) for 6 h (A) and RAW264.7 cells transfected with DTX3L shRNA or pLL3.7 vector, followed by RSV infection (MOI of 10) for 12 h (B). Ctrl, control (no infection). (C) HEK293T cells were cotransfected with Myc-TBK1, Flag-DTX3L full-length encoded plasmids, and HA-ubiquitin-K27, HA-ubiquitin-K48, or HA-ubiquitin-K63 plasmids for 48 h. Cellular lysates were immunoprecipitated with anti-Myc. Immunoprecipitates were analyzed by immunoblotting with anti-Myc and anti-HA. (D) HEK293T cells were cotransfected with expression plasmids for Myc-TBK1-WT or Myc-TBK1-K30R, Myc-TBK1-K401R, Myc-TBK1-K137R, or Myc-TBK1-K154R along with Flag-DTX3L and HA-ubiquitin-K63 plasmids. Cellular lysates were immunoprecipitated with anti-Myc. Immunoprecipitates were analyzed by immunoblotting with anti-Myc and anti-HA. Results are representative of at least three independent experiments.

DISCUSSION

At present, most reports on DTX3L are about its role in regulating cell cycle and tumor growth (24, 25). For example, DTX3L as an oncogenic survival factor mediating proliferation, chemo-resistance and survival of metastatic prostate cancer cells (26). In addition, DTX3L could promote the proliferation and cell adhesion-mediated drug resistance of myeloma cells (24). In our research, we found that DTX3L was a positive-

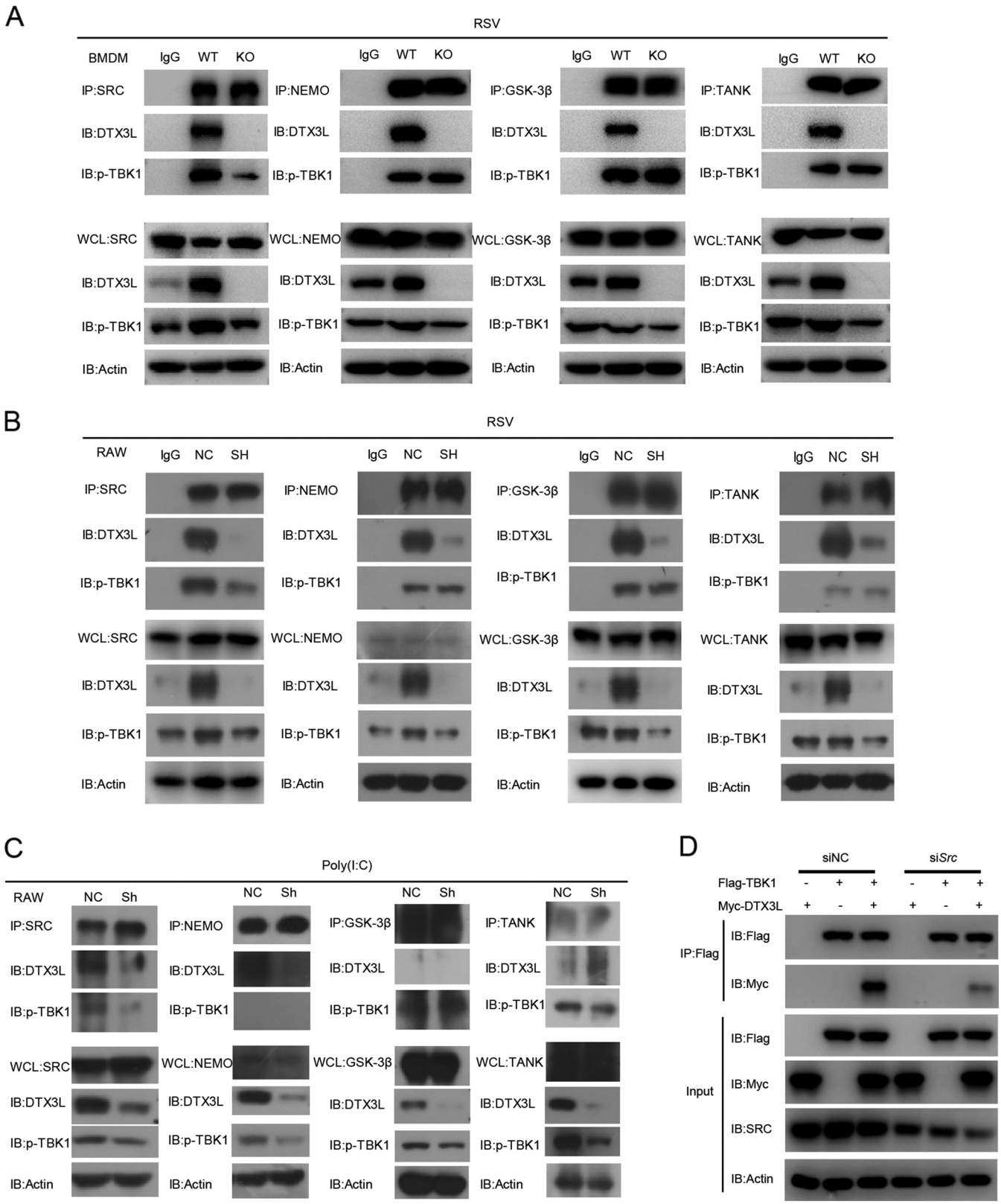

FIG 8 DTX3L promotes phosphorylation of TBK1 through SRC. (A) Immunoprecipitation and immunoblot analysis of SRC, NEMO, GSK-3β, or TANK and DTX3L and p-TBK1 in WT and *Dtx3l*$^{-/-}$ bone marrow-derived macrophage (BMDMs), followed by RSV infection (MOI of 10) for 12 h. Results are representative of at least three independent experiments. (B) Immunoprecipitation and immunoblot analysis of SRC, NEMO, GSK-3β, or TANK and DTX3L and p-TBK1 in RAW264.7 cells stably transduced with lentivirus encoding pLL3.7 vector or shRNA specific for DTX3L, followed by RSV infection (MOI of 10) for 12 h. Results are representative of at least three independent experiments. (C) Immunoprecipitation and immunoblot analysis of SRC, NEMO, GSK-3β, or

(Continued on next page)

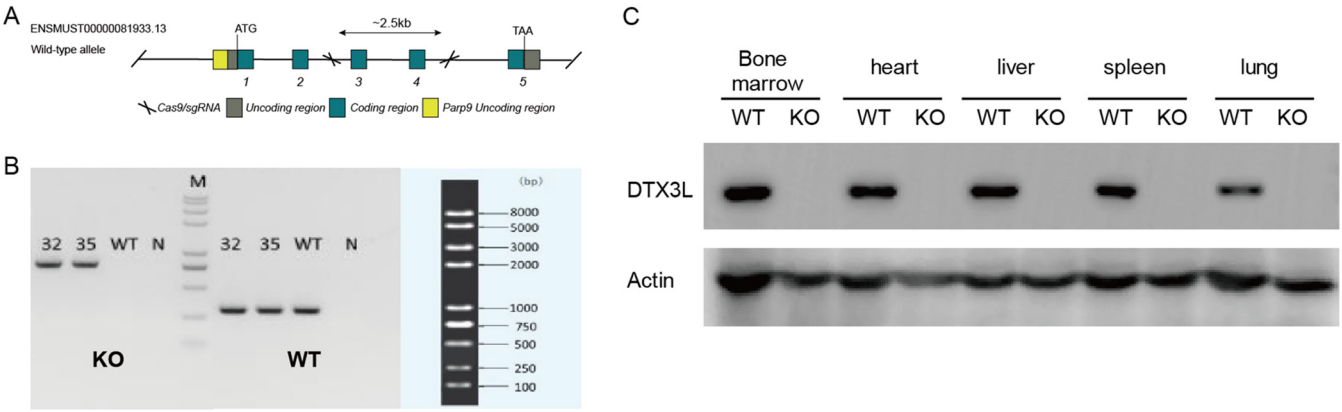

FIG 9 Generation and confirmation of *Dtx3l*$^{-/-}$ mice. (A) Generation and gene sequence insertion of *Dtx3l*$^{-/-}$ mice by CRISPR/Cas9 strategy; (B and C) confirmation of DTX3L knockout at the DNA (B) and protein (C) levels. Samples 32 and 35 in the left and right lanes correspond to *Dtx3l* KO and WT primer PCR results, respectively. In the lanes, WT is the C57BL/6J wild type, N is the negative blank control, and M represents the DNA ladder. Results are representative of at least three independent experiments.

feedback regulator of innate antiviral immunity, which enriches the known biological functions of DTX3L on regulating cell cycle and tumor growth.

Recently, some groups' studies reveal that DTX3L binds to ADP-ribosyltransferase PARP9 to form a heterodimer, which plays a role in DNA damage repair (27–29). It has been reported that DTX3L monoubiquitinates multiple histones, including histones H2A, H2B, H3, and H4 (30). DTX3L mediated the monoubiquitination of Lys-91 of histone H4 (H4K91UB1) during DNA damage (28). Our present study displays that after RSV infection in macrophages, DTX3L expression was increased to enhance the type I interferon signal and thereby control viral infection. *Dtx3l*$^{-/-}$ mice showed more severe lung inflammation and impaired interferon production in bone marrow-derived macrophages. Mechanically, after RSV infection, the transcription factor ETS1 translocated into the nucleus in the presence of IFNAR1, the *Dtx3l* promoter activity and the expression of DTX3L was upregulated in macrophages. DTX3L as an E3 ligase ubiquitinated K30 and K401 sites of TBK1 in K63-linked polyubiquitination way, confirming the new type of DTX3L-mediated ubiquitination. Therefore, as an E3 ubiquitin ligase, DTX3L may mediate ubiquitination at both the DNA and protein levels, regulating target protein homeostasis and promoting DNA repair and signal transduction.

It has been reported that the expression of DTX3L and PARP9 was significantly increased in STAT1 constitutively activated mouse and human fibrosarcoma U3A cells: the expression of DTX3L and PARP9 was regulated by interferon. It was found that after viral infection, DTX3L could ubiquitinate histone H2BJ and promote the expression of ISGs, thus enhancing the antiviral effect of cells (17). Here, we demonstrated that the expression of type I interferon decreased in DTX3L-deficient RAW264.7 cells, suggesting that DTX3L regulates the production of interferon, thereby promoting the expression of downstream ISGs. Particularly, we found RSV infection and IFN-β stimulation promoted nuclear translocation of the transcription factor ETS1, thereby enhancing *Dtx3l* promoter activity and DTX3L expression. Moreover, ETS1 increased expression of DTX3L stimulated by RSV depended on the presence of type I IFN. Thus, RSV-stimulated interferon promotes the translocation of ETS1 into the nucleus, thereby increasing DTX3L expression, after which positive feedback acts on the upstream of the interferon signaling pathway to promote interferon production. This finding enriches and complements the antiviral role of DTX3L in the interferon signaling pathway.

FIG 8 Legend (Continued)
TANK and DTX3L and p-TBK1 in RAW264.7 cells stably transduced with lentivirus encoding pLL3.7 vector or shRNA specific for DTX3L, followed by poly(I·C) stimulation for 8 h. (D) Control or *Src*-siRNA-transfected HEK293T cells were cotransfected with Myc-DTX3L and Flag-TBK1 full-length encoded plasmids and pcDNA3.1(−) plasmids, and cellular lysates were immunoprecipitated with anti-Flag 48 h later. Immunoprecipitation was analyzed by immunoblotting with anti-Flag and anti-Myc.

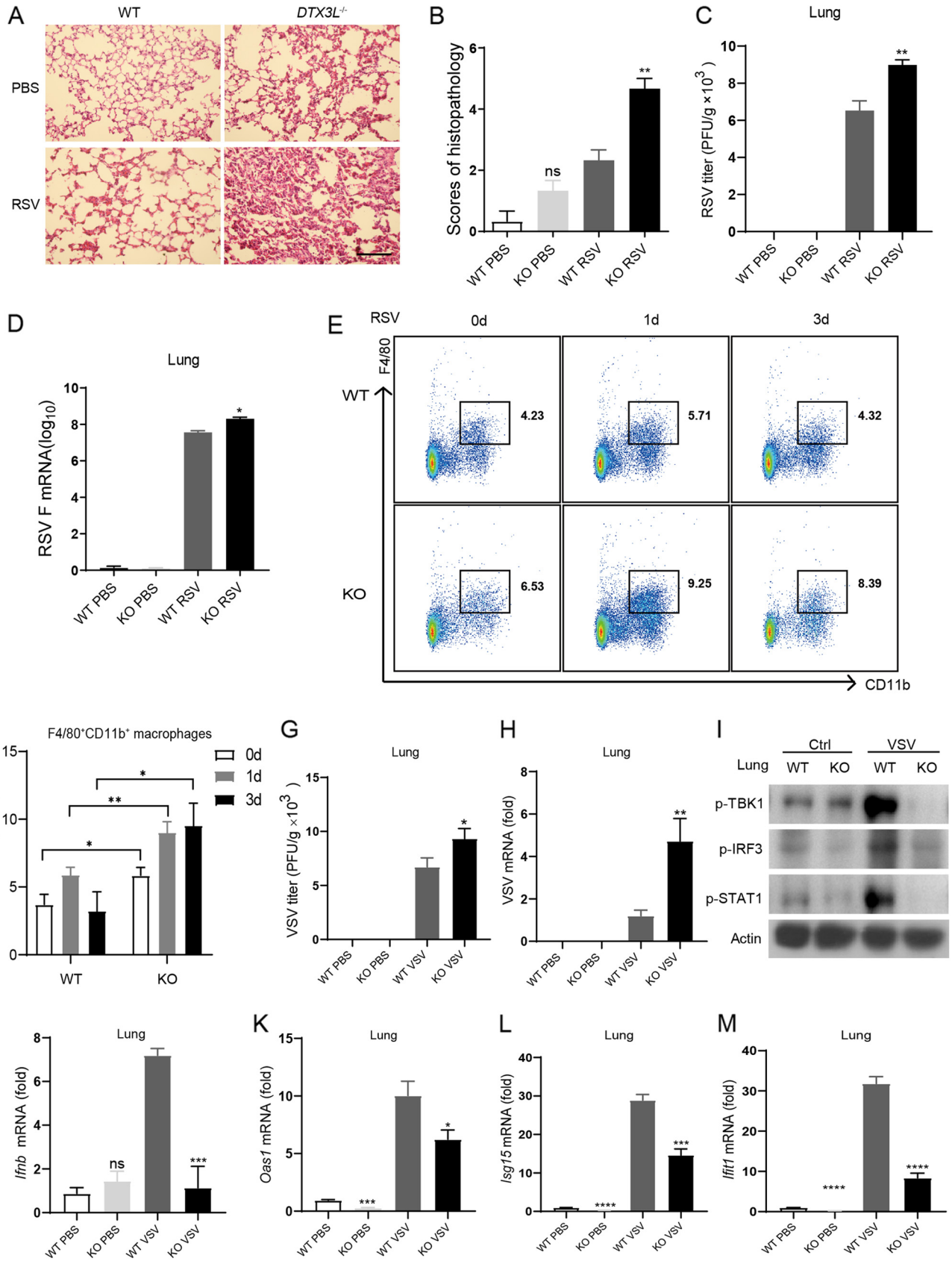

FIG 10 DTX3L knockout mice exhibited aggravated lung inflammation. (A) Hematoxylin and eosin staining (×200 magnifications) of lung tissues from WT and *Dtx3l*$^{-/-}$ mice infected with RSV (1×10^9 PFU per g [body wt] of mouse) intranasally. Scale bar, 100 μm. (B) Statistical analysis and histopathology

(Continued on next page)

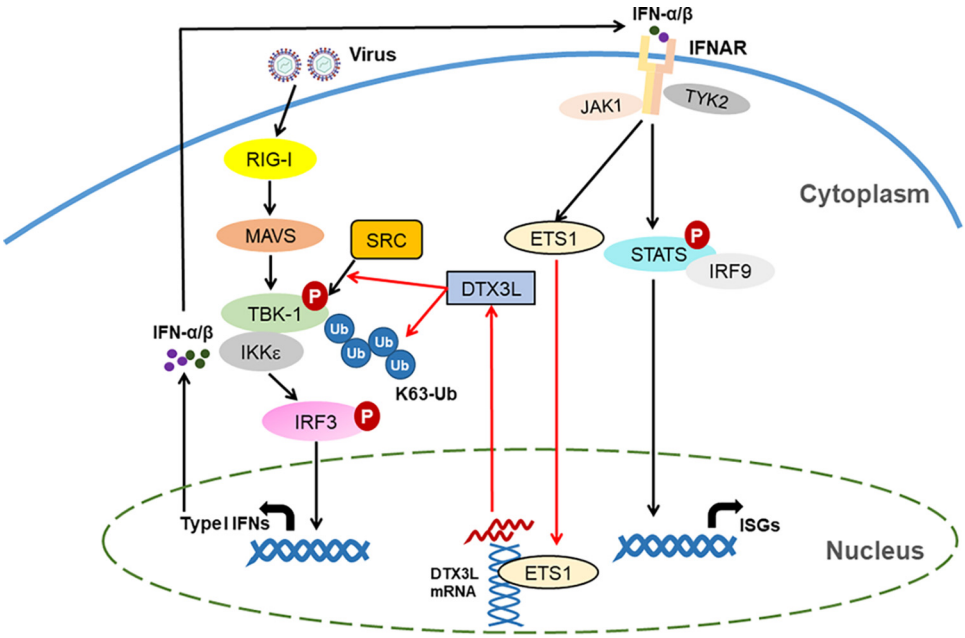

FIG 11 DTX3L enhances the type I interferon antiviral response. Shown is a proposed model depicting the role of DTX3L in positive regulation of IFN-I production during virus infection. RSV and IFN-β enhance the translocation of ETS1 to the nucleus to promote the expression of DTX3L. DTX3L as an E3 ligase ubiquintinates TBK1 at K30 and K401 in the K63-linked polyubiquitination pathway and promotes the phosphorylation of TBK1 through binding with kinase SRC, leading to the increased activation of TBK1 and production of IFNs and IFN-stimulated genes (ISGs), which limits virus infection.

The activation of TBK1 requires a variety of ways, including homodimerization, ubiquitination, and phosphorylation, which stimulates translocation of IRF3 (19, 23). Our study defined DTX3L as a positive regulator of K63-linked ubiquitination of TBK1. In addition, we found DTX3L could also promote the phosphorylation of TBK1. Four phosphokinases (SRC, NEMO, TANK, and GSK-3β) that regulate TBK1 phosphorylation were screened, and we learned that DTX3L could promote TBK1 phosphorylation by binding phosphokinase SRC. These findings revealed an important regulation of the interaction between DTX3L and TBK1. Thus, we provide evidence that DTX3L regulates type I IFN signaling through IFN-β–ETS1–DTX3L–TBK1 positive-feedback loop during RSV infection in addition to its well-studied function in the STAT1-actived cells (17).

In this study, we identify DTX3L as an antiviral molecule by promoting IFN production and establishing a IFN-β–ETS1–DTX3L–TBK1 positive-feedback loop as a novel immunomodulatory step to enhance interferon signaling and inhibit RSV infection. Whether other types of virus also promote the expression of DTX3L and depend on DTX3L regulating TBK1 activation and IFN expression for antiviral activity still needs to be determined. Nonetheless, small-molecule-targeted drugs that mimic the antiviral mechanism of DTX3L should help to fill the unmet need for protection against the lung diseases such as bronchiolitis and pneumonia that develop with RSV and perhaps the need for the treatment of other interferon-sensitive conditions.

FIG 10 Legend (Continued)
scores of hematoxylin and eosin staining of lung tissue. (C) The lung RSV titer at day 3 after intranasal infection was determined by plaque assay. Data represent mean values of RSV PFU per gram of lung tissue. (D) Expression of RNA encoding RSV fusion protein (RSV F) in lung tissues of WT and *Dtx3l*$^{-/-}$ mice infected with RSV (1×10^9 PFU per g [body wt] of mouse) by intranasal injection. (E) Peripheral blood mononuclear cells (PBMCs) were isolated from WT and *Dtx3l*$^{-/-}$ mice infected with VSV (1×10^8 PFU per g [body wt] of mouse) by intranasal injection for 24 h. Macrophage subsets were analyzed by flow cytometry after staining for F4/80 and CD11b. $n = 3$ per group. (F) The percentages of F4/80$^+$ CD11b$^+$ macrophages were higher in the PBMCs of *Dtx3l*$^{-/-}$ mice than in WT mice. $n = 3$ per group. (G) The lung VSV titer at 24 h after intranasal infection was determined by plaque assay. Data represent mean values of RSV PFU per gram of lung tissue. (H) qPCR analysis of VSV viral RNA in the lung tissues from WT and *Dtx3l*$^{-/-}$ mice infected with VSV (1×10^8 PFU per g [body wt] of mouse) by intranasal injection for 24 h; (I) immunoblot analysis of p-TBK1, p-IRF3, and p-STAT1 in the lung tissues from WT and *Dtx3l*$^{-/-}$ mice infected with VSV (1×10^8 PFU per g [body wt] of mouse) by intranasal injection for 24 h. (J to M) qPCR analysis of *Ifnb* (J), *Oas1* (K), *Isg15* (L), and *Ifit1* (M) mRNA in the lung tissues from WT and *Dtx3l*$^{-/-}$ mice infected with VSV (1×10^8 PFU per g [body wt] of mouse) by intranasal injection for 24 h. All qPCR results are represented as relative fold changes after normalization to *Gapdh* controls. Results are expressed as mean ± SEM and are representative of at least three independent experiments. ns, not significant ($P > 0.05$); **, $P < 0.01$; ***, $P < 0.001$.

TABLE 1 CRISPR/Cas9 gRNA sequences

gRNA name	gRNA sequence (5′→3′)	PAM[a]
gRNA1	AACGCTAGGCGACTCCATCT	TGG
gRNA2	GCTTGACCCTTGAGGACTAA	GGG
gRNA3	CTTCTACCCTGCCATTCATA	AGG
gRNA4	AACTTGGGTAGTATTCATCT	TGG

[a]PAM, protospacer-adjacent motif.

MATERIALS AND METHODS

Mice. The generation of DTX3L knockout mice (C57BL/6) was conducted at GemPharmatech Co., Ltd., Nanjing, China, using CRISPR/Cas9 technology. Guide RNA (gRNA) was designed and transcribed *in vitro*; the gRNA sequences are listed in Table 1. Cas9 and gRNA were simultaneously injected into fertilized mice eggs. Under the guidance of gRNA, the Cas9 protein binds to the target site and causes DNA double-strand breaks, thereby achieving deletion of the base sequence of the target site. Exons 3 to 4 of the *Dtx3l* gene were selected as the knockout region, and a total of 1,742 bp was knocked out. Knocking out this region would cause frameshift mutations in the open reading frame and premature termination of translation, thus leading to protein mutation. Final realization and gene knockout are shown in Fig. 7A to C. Wild-type (WT) C57BL/6 mice were purchased from Shanghai SLAC Laboratory Animal Co., Ltd. Genotyping of WT and knockout (KO) mice was performed with the following primers: KO forward (For), 5′-TGATGGAGGTGTGGGAAAGACTG-3′, and KO reverse (Rev), 5′-GGAATCAAAGCCATGCTGGAGAG-3′; and WT For, 5′-ATGGAGATCAGCAGGAGAATGCAG-3′, and WT Rev, 5′-ATGGTGCCACAGCCTTCATAACC-3′. IFNAR1$^{-/-}$ (type I IFN receptor KO) mice were gifts from Chunsheng Dong of Institutes of Biology and Medical Sciences (Soochow University, Suzhou, China). All mice were maintained under specific-pathogen-free (SPF) conditions in the animal facility of Soochow University.

Cell culture and reagents. RAW264.7, HEK293T, B16, NIH 3T3, and Hep2 cells were purchased from the American Type Culture Collection (ATCC) and were cultured in Dulbecco's modified Eagle's medium (DMEM) (HyClone) supplemented with 10% fetal bovine serum (FBS) (Biological Industries), 100 U/mL penicillin (NCM Biotech), and 100 μg/mL streptomycin (NCM Biotech) at 37°C under 5% CO_2. Recombinant mouse IFN-β (mIFN-β) was purchased from R&D Systems. Poly(I·C) was purchased from Merck. Purified anti-mouse IFNAR1 antibody (MAR1-5A3) and purified mouse IgG1 antibody (MOPC-21) were purchased from BioLegend.

Primary cells from mice. Mouse tissues were prepared from 6- to 8-week-old mice (WT or *Dtx3l*$^{-/-}$) and were cut into pieces and ground into the cell suspension briefly on the ice. Mouse primary heart, liver, spleen, and lung cells were collected and prepared for further experiments. Bone marrow-derived macrophages (BMDMs) were generated from the bone marrow of 6- to 8-week-old mice. Bone marrow cells were collected from the femurs and tibias of mice, and BMDMs were differentiated in RPMI 1640 medium with 10% FBS, including 20 ng/mL mouse macrophage colony-stimulating factor (M-CSF) (Pepro Tech, Rocky Hill, NJ) and 20 ng/mL mouse granulocyte-macrophage colony-stimulating factor (GM-CSF) (Pepro Tech, Rocky Hill, NJ). Mouse primary peritoneal macrophages were prepared from 6- to 8-week-old C57BL/6J mice through intraperitoneal injection with 4% thioglycolate (Invitrogen) for 4 days.

RNA knockdown and plasmid transfection. siRNA knockdown of Src in HEK293T cells and Ets1 in NIH 3T3 cells by GP-transfect-Mate siRNA transfection reagent (siRNA concentration, 10 nM) were handled following the manufacturer's protocols. As a negative control, a nontargeting scrambled siRNA pool (control siRNA) was used at the same concentration. HA-tagged ubiquitin (HA-Ub), HA-K27 (with all lysines on the ubiquitin gene mutated to arginines except K27), HA-K48 (with all lysines on the ubiquitin gene mutated to arginines except K48), and HA-K63 (with all lysines on the ubiquitin gene mutated to arginines except K63) plasmids were gifts from Hui Zheng of Institutes of Biology and Medical Sciences (Soochow University, Suzhou, China). His-SRC- and ETS-1-encoding plasmids were purchased from Fenghuishengwu. Mouse Flag-DTX3L cDNA was amplified from RNA of RAW264.7 cells using the following primers: For, 5′-CGCGGATCCGCCACCATGGCTTCCAGTCCCGACCC-3′; and Rev, 5′-CGGGGTACCTTAC TTGTCATCGTCGTCCTTGTAATCCTCAATGCCTTTTGCTTTCAGCT -3′. Mouse Myc-TBK1 cDNA was amplified from RNA of RAW264.7 cells using the following primers: For, 5′-CCGGAATTCGCCACCATGCAGAGCACC TCCAACCAT-3′; and Rev, 5′-CGGGGTACCCTACAGATCCTCTTCTGAGATGAGTTTTTGTTCAAGACAGTCCAC ATTGCGAAGG -3′. For the DTX3L knockdown plasmid, three pairs of siRNAs were designed by Thermal Fisher website siRNA design software (Table 2), and then the oligonucleotide sequence was synthesized by adding a specific ring structure sequence and restriction site. Then, PCR annealing was performed with the following procedure: 95°C for 30 s, followed by 72°C for 2 min, 37°C for 2 min, 25°C for 2 min, and then hold at 4°C. Myc-TBK1 K30, K401, K137, and K154 mutants were generated by GENEWIZ. All transient transfections were carried out using d-Portal transfection reagent according to the manufacturer's instructions.

Virus preparation, titration, and infection. The RSV viral stock (L19 strain) was obtained from Chunsheng Dong of Institutes of Biology and Medical Sciences (Soochow University, Suzhou, China) and was grown in Hep2 cells. Vesicular stomatitis virus (VSV) and Sendai virus (SeV) were gifts from Hui Zheng, Institutes of Biology and Medical Sciences (Soochow University, Suzhou, China). Titers of viable virus were determined by plaque assay (31). The plaque assay was performed with a standard culture infectious dose assay on Vero cell monolayers in 96-well plates with virus dilutions. After virus infection, the plates were incubated for the indicated times. The medium was then removed, and the cells were fixed with 4% paraformaldehyde for 15 min and stained with 1% crystal violet for 30 min before plaque counting. After being washed twice with 1× phosphate-buffered saline (PBS), RAW264.7 cells or BMDMs

TABLE 2 DTX3L shRNA sequences

siRNA primer	Sequence (5′→3′)
DTX3L shRNA1 F	TGGATGAAGCACTTTGTGATGATTCAAGAGATCATCACAAAGTGCTTCATCCTTTTTTC
DTX3L shRNA1 R	TCGAGAAAAAAGGATGAAGCACTTTGTGATGATCTCTTGAATCATCACAAAGTGCTTCATCCA
DTX3L shRNA2 F	TGCTGCTTCCCAAAGCTCTTGATTCAAGAGATCAAGAGCTTTGGGAAGCAGCTTTTTTC
DTX3L shRNA2 R	TCGAGAAAAAAGCTGCTTCCCAAAGCTCTTGATCTCTTGAATCAAGAGCTTTGGGAAGCAGCA
DTX3L shRNA3 F	TGCCTGAACTGCTCCAGGAAATTTCAAGAGAATTTCCTGGAGCAGTTCAGGCTTTTTTC
DTX3L shRNA3 R	TCGAGAAAAAAGCCTGAACTGCTCCAGGAAATTCTCTTGAAATTTCCTGGAGCAGTTCAGGCA

were challenged with RSV (multiplicity of infection [MOI] of 10), VSV (MOI of 1), or SeV (MOI of 1) in 2% medium for 2 h for virus entry. Then, the infection medium was removed by being washed twice with 1× PBS. Cells were fed in the fresh 10% FBS medium for the indicated times. Then, the cells were analyzed by quantitative real-time PCR (qPCR) or Western blotting. For *in vivo* viral infection studies, 6- to 8-week-old mice (WT or *Dtx3l*$^{-/-}$) were lightly anesthetized with 4% chloral hydrate before intranasal inoculation with 1×10^9 PFU of RSV in 2% DMEM or PBS. Five days after infection, lung tissue and bone marrow were harvested for qPCR, Western blotting, and lung histology.

RNA isolation and quantitative real-time PCR. Total RNAs were isolated from cell lines or mouse tissues using RNA-easy isolation reagent (Vazyme). The cDNA was synthesized from 1 μg of total RNA using a HIScript III 1st strand cDNA synthesis kit (Vazyme) and subjected to qPCR with different primers in the presence of SYBR green supermix (Yeasen) using the Eppendorf qPCR system. The relative expression of the target genes was normalized to GAPDH (glyceraldehyde-3-phosphate dehydrogenase) mRNA. The sequences for primers are listed in Table 3.

Mass spectrometry analysis. RAW264.7 cells were infected or uninfected with RSV for 24 h and then sonicated three times on ice using a high-intensity ultrasonic processor (Scientz) in lysis buffer containing 150 mM NaCl, 10 mM HEPES, 8 M urea, and protease inhibitor mixtures (Sigma). The remaining debris was removed by centrifugation at 12,000 × *g* at 4°C for 10 min. Finally, the supernatant was collected and the protein concentration was determined with a bicinchoninic acid (BCA) kit according to the manufacturer's instructions (Thermo Fisher). For digestion, the protein solution was treated with 5 mM dithiothreitol for 30 min at 56°C and alkylated with 11 mM iodoacetamide for 15 min at room temperature in darkness. Finally, trypsin (Thermo Fisher) was added at 1:50 trypsin-to-protein mass ratio overnight. The tryptic peptides were purified using C_{18} Zip Tip. Then, the peptides were analyzed by an Orbitrap Elite hybrid mass spectrometer (Thermo Fisher) coupled with a Dionex liquid chromatography (LC) device. The resulting MS/MS data were processed using Proteome Discoverer 1.2. Tandem mass spectra were searched against UniProt database concatenated with a reverse decoy database. The mass tolerance for fragment ions was set as 0.02 Da. Systematic bioinformatics analysis of proteins, including protein annotation, function classification, function enrichment was conducted.

Flow cytometry. Cells were stained with fluorescence-coupled antibodies diluted in PBS for 20 min on ice and subsequently washed with PBS. Analysis was carried out on BD Cyan (BD Biosciences, USA). Fluorescein isothiocyanate (FITC)-conjugated anti-F4/80 (QA17A29; no. 157302) and phycoerythrin (PE)-conjugated anti-CD11b (M1/70; no. 101208) were purchased from BioLegend (San Diego, CA, USA).

Immunoblotting and immunoprecipitation. Cells were harvested using NP-40 lysis buffer (Beyotime) and phenylmethylsulfonyl fluoride (PMSF) (Beyotime). After centrifugation at 12,000 rpm for 20 min, protein concentrations were measured, and equal amounts of lysates were used for immunoblotting and immunoprecipitation. Immunoprecipitation was performed using specific antibodies at 4°C. Protein G/A agarose beads (Roche Diagnostics GmbH) were added to samples, and the mixtures were incubated on a rotor at 4°C for 4 h. After being washed twice with NP-40 washing buffer and once with high-salt washing buffer, the

TABLE 3 Quantitative real-time PCR and primers

	Sequence (5′→3′)	
Gene	Forward primer	Reverse primer
RSV F	GAATTGCAGTTGCTCATGCAA	TGGCGATTGCAGATCCAACA
RSV N	CATCTAGCAAATACACCATCCA	TTCTGCACATCATAATTAGGAGTATCAA
Dtx3l	GGTCTCTGGATGAAGCACTT	AGAGAGCAGGTCACAGTTCA
Ifit2	GACACAGCAGACAGTTACAC	GTATGTTGCACATGGTGGCT
Iigp1	AAGAGCCTGTAGCAGTGAAG	AGGTGAAGAGAACAGCTGAC
Rnf213	TCGTTGTCTGCGAGTTGTCT	TGCAGGTTGATGTCACTCCA
Pclaf	GTCACCAATTCTTCAAGTTCG	TTCCTAAGCCACTGGTTCCT
Ifna	GCCTTAACCCTCCTGGTAAAA	TCCTGTGGGAATCCAAAGTC
Ifnb	ATGAGTGGTGGTTGCAGGC	TGACCTTTCAAATGCAGTAGATTCA
Ifit1	AGAAACCTGCCAAGTATGATGACA	GGAAGAGTGGGAGTTGCTGTTG
Oas1	CCCTATCTGACACATTAGCGGT	ATATCTATGGTCCCCCAGCCT
Isg15	CGATTTCCTGGTGTCCGTGA	AGCCAGAACTGGTCTTCGTG
Ets1	CTGTTAACTCCGAGCAGCAA	CAGGCTGAACTCATTCACAG
Gapdh	AGAAACCTGCCAAGTATGATGACA	GGAAGAGTGGGAGTTGCTGTTG

immunoprecipitates were eluted by boiling with the loading buffer containing β-mercaptoethanol for 10 min and analyzed by SDS-PAGE, followed by transfer to polyvinylidene difluoride (PVDF) membranes. Membranes were then blocked with 5% nonfat milk for 1 h at room temperature and then probed with the primary antibodies, followed by incubation with the anti-mouse or anti-rabbit (Proteintech) secondary antibodies. Immunoreactive bands were visualized in the dark room with Clarity Western ECL enhanced chemiluminescence substrate (Bio-Rad). The antibodies with the indicated dilutions according to the manufacturer's protocol were as follows: DTX3L (LS-C287683; LSBio; 1:5000), TBK1 (no. 38066; Cell Signaling Technology;1:1000), p-TBK1 (no. 5483; Cell Signaling Technology; 1:1000), Rig-I (no. 3743; Cell Signaling Technology;1:1000), MAVS (no. 24930; Cell Signaling Technology;1:1000), Flag (no. T0003; Affinity; 1:5000), HA (no. 3724; Cell Signaling Technology; 1:1000), Myc (no. 2276; Cell Signaling Technology; 1:1000), TANK (no. 2141; Cell Signaling Technology; 1:1000), Src (no. 2109; Cell Signaling Technology; 1:1000), GSK-3β (no. 12456; Cell Signaling Technology; 1:1000), β-actin (no. T0022; Affinity; 1:50000), ubiquitin (Ub) (no. 3936; Cell Signaling Technology; 1:1000), STAT1 (sc-464; Santa Cruz; 1:500), and ETS-1 (no. 14069; Cell Signaling Technology; 1:2000).

Native PAGE. Native PAGE for the detection of IRF3 dimerization was performed on acrylamide gel without SDS. Cells were lysed with NP-40 lysis buffer (Beyotime) containing PMSF (Beyotime) and protease inhibitor cocktail (Roche). After centrifugation at 12,000 $\times$ *g* for 20 min, proteins in the supernatant were quantified. The gel was prerun for 30 min at 40 mA on ice with 25 mM Tris-HCl (pH 8.4) and 192 mM glycine with 1% deoxycholate in the cathode chamber. The unboiled total protein was added to the gel for 80 min at 25 mA on ice, and the proteins were transferred to PVDF membranes for immunoblot analysis.

Immunofluorescence. Primary peritoneal macrophages (WT or IFNAR1$^{-/-}$) plated on glass coverslips in eight-well plates were infected with RSV for 0, 6, or 12 h or stimulated with IFN-β for 0, 2, or 4 h. Cells were fixed with 4% paraformaldehyde for 1 h at room temperature, permeabilized using 0.2% Triton X-100, blocked with 3% bovine serum albumin (BSA) in PBS for 1 h, and stained with rabbit anti-ETS1 (no. 14069; Cell Signaling Technology), rabbit anti-DTX3L (LS-C287683; LSBio), or mouse anti-TBK1 (A-6; Santa Cruz Biotechnology), followed by staining with Alexa Fluor 488-labeled anti-rabbit secondary antibody (Southern Biotech) or Texas Red-labeled anti-mouse secondary antibody (Invitrogen) to detect colocalization of DTX3L and TBK1 or location of ETS1.The nuclei were stained with DAPI (4′,6-diamidino-2-phenylindole) (Roche). Images were captured and analyzed with a Nikon A1 confocal microscope.

Luciferase reporter assay. B16 cells were cotransfected with *Ifnb* promoter reporter plasmid and DTX3L and RIG-IN expression or control vector plasmid. Forty-eight hours later, cells were infected with RSV (MOI of 1) for 12 h, and the luciferase activity was detected by a dual-luciferase reporter assay system (GN201-01; Yuanpinghao Biology) according to the manufacturer's protocol. HEK293 cells were cotransfected with *Dtx3l* promoter reporter plasmid, together with the ETS1 expression or control vector plasmid. Forty-eight hours later, the luciferase activity was determined.

Lung histology. Lungs from control or virus-infected mice (WT or *Dtx3l*$^{-/-}$) were collected, fixed in 10% phosphate-buffered formalin, embedded in paraffin wax, and sectioned at a thickness of 5 μm. The sections were stained with hematoxylin and eosin solution (H&E) and examined and images captured by light microscopy (Nikon Eclipse TE2000-S microscope) for histological changes. The histopathology scores were completed by two researchers independently. According to the method of Roderick et al. (32), the thickening of alveolar wall, the infiltration of inflammatory cells, and the degree of damage of lung tissue structure were scored. The results of three experiments were taken for statistical analysis.

Statistical analysis. All data were analyzed from three independent experiments and are presented as the mean $\pm$ standard error of the mean (SEM). The significance of difference between groups was determined by two-tailed Student's *t* test and one-way analysis of variance. Figures and statistical analysis were generated using GraphPad Prism 5. *P* values of <0.05 were considered statistically significant: *, $P < 0.05$; **, $P < 0.01$; ***, $P < 0.001$.

Study approval. All animal experiments were undertaken in accordance with the National Institutes of Health *Guide for the Care and Use of Laboratory Animals* (33) with approval by Soochow University, Suzhou. All animal experiment procedures have been reviewed and approved by the Animal Ethical Committee of Soochow University (SYXK2015-0018).

Data availability. The mass spectrometry proteomics data have been deposited in the ProteomeXchange Consortium via the PRIDE (34) partner repository under the data set identifier PXD042041.

ACKNOWLEDGMENTS

This work was supported by grants from the National Natural Science Foundation of China (grant no. 82270018, 82170012, 81771667, 31800736, 81970027, 81770115, 82070009, and 82071765), Suzhou Medical Youth Talent Project (grant no. GSWS2019047; GSWS2020053), Natural Science Foundation of Jiangsu Province to Yi Yang (grant no. BK20170349), Social Development Project of Jiangsu Province (grant no. BE2021656, BE2019671, and BE2016676), Program for Changjiang Scholars and Innovative Research Team in University (grant no. PCSIRT and IRT1075), and Jiangsu Key Laboratory of Infection and Immunity, Institutes of Biology and Medical Sciences of Soochow University, Key Lab of Respiratory Disease of Suzhou (grant no. SZS201714), and Key Laboratory for Diagnosis and Treatment of Immune Diseases in Children (grant no. SZS201808), as well as a Translational Research Grant of NCRCH (grant no. 2020ZKZC04) and the Postgraduate Research & Practice Innovation Program of Jiangsu Province (KYCX20_2723).

Chuangli Hao, Jinping Zhang, Zhengrong Chen, and Yi Yang conceived and supervised the study. Jiaqi Huang performed most of the experiments and wrote the manuscript. Yunfei Ye, Yu Shao, and Xiaoping Li prepared the figures and performed part of the cell and mouse experiments. Peijie Zhu, Yu Ma, Fei Xu, and Ji Zhou assisted with the reagent preparation, transfections, lentivirus, and coimmunoprecipitation experiments. Mengyun Wu and Xiu Gao performed part of the molecular mechanism experiments. All authors approved the final version of the paper.

We declare no conflict of interest.

REFERENCES

1. Bryce J, Boschi-Pinto C, Shibuya K, Black RE, WHO Child Health Epidemiology Reference Group. 2005. WHO estimates of the causes of death in children. Lancet 365:1147–1152. https://doi.org/10.1016/S0140-6736(05)71877-8.
2. Rudan I, Boschi-Pinto C, Biloglav Z, Mulholland K, Campbell H. 2008. Epidemiology and etiology of childhood pneumonia. Bull World Health Organ 86:408–416. https://doi.org/10.2471/blt.07.048769.
3. Xing Y, Proesmans M. 2019. New therapies for acute RSV infections: where are we? Eur J Pediatr 178:131–138. https://doi.org/10.1007/s00431-018-03310-7.
4. Sadler AJ, Williams BR. 2008. Interferon-inducible antiviral effectors. Nat Rev Immunol 8:559–568. https://doi.org/10.1038/nri2314.
5. Streicher F, Jouvenet N. 2019. Stimulation of innate immunity by host and viral RNAs. Trends Immunol 40:1134–1148. https://doi.org/10.1016/j.it.2019.10.009.
6. Randall RE, Goodbourn S. 2008. Interferons and viruses: an interplay between induction, signalling, antiviral responses and virus countermeasures. J Gen Virol 89:1–47. https://doi.org/10.1099/vir.0.83391-0.
7. Jewell NA, Vaghefi N, Mertz SE, Akter P, Peebles RS, Jr, Bakaletz LO, Durbin RK, Flano E, Durbin JE. 2007. Differential type I interferon induction by respiratory syncytial virus and influenza a virus in vivo. J Virol 81:9790–9800. https://doi.org/10.1128/JVI.00530-07.
8. Bhoj VG, Sun Q, Bhoj EJ, Somers C, Chen X, Torres JP, Mejias A, Gomez AM, Jafri H, Ramilo O, Chen ZJ. 2008. MAVS and MyD88 are essential for innate immunity but not cytotoxic T lymphocyte response against respiratory syncytial virus. Proc Natl Acad Sci U S A 105:14046–14051. https://doi.org/10.1073/pnas.0804717105.
9. Demoor T, Petersen BC, Morris S, Mukherjee S, Ptaschinski C, De Almeida Nagata DE, Kawai T, Ito T, Akira S, Kunkel SL, Schaller MA, Lukacs NW. 2012. IPS-1 signaling has a nonredundant role in mediating antiviral responses and the clearance of respiratory syncytial virus. J Immunol 189:5942–5953. https://doi.org/10.4049/jimmunol.1201763.
10. Schijf MA, Lukens MV, Kruijsen D, van Uden NO, Garssen J, Coenjaerts FE, Van't Land B, van Bleek GM. 2013. Respiratory syncytial virus induced type I IFN production by pDC is regulated by RSV-infected airway epithelial cells, RSV-exposed monocytes and virus specific antibodies. PLoS One 8:e81695. https://doi.org/10.1371/journal.pone.0081695.
11. Goritzka M, Makris S, Kausar F, Durant LR, Pereira C, Kumagai Y, Culley FJ, Mack M, Akira S, Johansson C. 2015. Alveolar macrophage-derived type I interferons orchestrate innate immunity to RSV through recruitment of antiviral monocytes. J Exp Med 212:699–714. https://doi.org/10.1084/jem.20140825.
12. Hijano DR, Vu LD, Kauvar LM, Tripp RA, Polack FP, Cormier SA. 2019. Role of type I interferon (IFN) in the respiratory syncytial virus (RSV) immune response and disease severity. Front Immunol 10:566. https://doi.org/10.3389/fimmu.2019.00566.
13. Song Y, Lai L, Chong Z, He J, Zhang Y, Xue Y, Xie Y, Chen S, Dong P, Chen L, Chen Z, Dai F, Wan X, Xiao P, Cao X, Liu Y, Wang Q. 2017. E3 ligase FBXW7 is critical for RIG-I stabilization during antiviral responses. Nat Commun 8:14654. https://doi.org/10.1038/ncomms14654.
14. Liu H, Li M, Song Y, Xu W. 2018. TRIM21 restricts coxsackievirus B3 replication, cardiac and pancreatic injury via interacting with MAVS and positively regulating IRF3-mediated type-I interferon production. Front Immunol 9:2479. https://doi.org/10.3389/fimmu.2018.02479.
15. Song G, Liu B, Li Z, Wu H, Wang P, Zhao K, Jiang G, Zhang L, Gao C. 2016. E3 ubiquitin ligase RNF128 promotes innate antiviral immunity through K63-linked ubiquitination of TBK1. Nat Immunol 17:1342–1351. https://doi.org/10.1038/ni.3588.
16. Wang C, Chen T, Zhang J, Yang M, Li N, Xu X, Cao X. 2009. The E3 ubiquitin ligase Nrdp1 'preferentially' promotes TLR-mediated production of type I interferon. Nat Immunol 10:744–752. https://doi.org/10.1038/ni.1742.
17. Zhang Y, Mao D, Roswit WT, Jin X, Patel AC, Patel DA, Agapov E, Wang Z, Tidwell RM, Atkinson JJ, Huang G, McCarthy R, Yu J, Yun NE, Paessler S, Lawson TG, Omattage NS, Brett TJ, Holtzman MJ. 2015. PARP9-DTX3L ubiquitin ligase targets host histone H2BJ and viral 3C protease to enhance interferon signaling and control viral infection. Nat Immunol 16:1215–1227. https://doi.org/10.1038/ni.3279.
18. Dwyer J, Li H, Xu D, Liu JP. 2007. Transcriptional regulation of telomerase activity: roles of the the Ets transcription factor family. Ann N Y Acad Sci 1114:36–47. https://doi.org/10.1196/annals.1396.022.
19. Tu D, Zhu Z, Zhou AY, Yun CH, Lee KE, Toms AV, Li Y, Dunn GP, Chan E, Thai T, Yang S, Ficarro SB, Marto JA, Jeon H, Hahn WC, Barbie DA, Eck MJ. 2013. Structure and ubiquitination-dependent activation of TANK-binding kinase 1. Cell Rep 3:747–758. https://doi.org/10.1016/j.celrep.2013.01.033.
20. Shu C, Sankaran B, Chaton CT, Herr AB, Mishra A, Peng J, Li P. 2013. Structural insights into the functions of TBK1 in innate antimicrobial immunity. Structure 21:1137–1148. https://doi.org/10.1016/j.str.2013.04.025.
21. Lei CQ, Zhong B, Zhang Y, Zhang J, Wang S, Shu HB. 2010. Glycogen synthase kinase 3beta regulates IRF3 transcription factor-mediated antiviral response via activation of the kinase TBK1. Immunity 33:878–889. https://doi.org/10.1016/j.immuni.2010.11.021.
22. Li X, Yang M, Yu Z, Tang S, Wang L, Cao X, Chen T. 2017. The tyrosine kinase Src promotes phosphorylation of the kinase TBK1 to facilitate type I interferon production after viral infection. Sci Signal 10:eaae0435. https://doi.org/10.1126/scisignal.aae0435.
23. Larabi A, Devos JM, Ng SL, Nanao MH, Round A, Maniatis T, Panne D. 2013. Crystal structure and mechanism of activation of TANK-binding kinase 1. Cell Rep 3:734–746. https://doi.org/10.1016/j.celrep.2013.01.034.
24. Shen Y, Sun Y, Zhang L, Liu H. 2017. Effects of DTX3L on the cell proliferation, adhesion, and drug resistance of multiple myeloma cells. Tumour Biol 39:1010428317703941. https://doi.org/10.1177/1010428317703941.
25. Camicia R, Winkler HC, Hassa PO. 2015. Novel drug targets for personalized precision medicine in relapsed/refractory diffuse large B-cell lymphoma: a comprehensive review. Mol Cancer 14:207. https://doi.org/10.1186/s12943-015-0474-2.
26. Bachmann SB, Frommel SC, Camicia R, Winkler HC, Santoro R, Hassa PO. 2014. DTX3L and ARTD9 inhibit IRF1 expression and mediate in cooperation with ARTD8 survival and proliferation of metastatic prostate cancer cells. Mol Cancer 13:125. https://doi.org/10.1186/1476-4598-13-125.
27. Takeyama K, Aguiar RC, Gu L, He C, Freeman GJ, Kutok JL, Aster JC, Shipp MA. 2003. The BAL-binding protein BBAP and related Deltex family members exhibit ubiquitin-protein isopeptide ligase activity. J Biol Chem 278:21930–21937. https://doi.org/10.1074/jbc.M301157200.
28. Yan Q, Dutt S, Xu R, Graves K, Juszczynski P, Manis JP, Shipp MA. 2009. BBAP monoubiquitylates histone H4 at lysine 91 and selectively modulates the DNA damage response. Mol Cell 36:110–120. https://doi.org/10.1016/j.molcel.2009.08.019.
29. Yan Q, Xu R, Zhu L, Cheng X, Wang Z, Manis J, Shipp MA. 2013. BAL1 and its partner E3 ligase, BBAP, link poly(ADP-ribose) activation, ubiquitylation, and double-strand DNA repair independent of ATM, MDC1, and RNF8. Mol Cell Biol 33:845–857. https://doi.org/10.1128/MCB.00990-12.
30. Yang C-S, Jividen K, Spencer A, Dworak N, Ni L, Oostdyk LT, Chatterjee M, Kuśmider B, Reon B, Parlak M, Gorbunova V, Abbas T, Jeffery E, Sherman NE, Paschal BM. 2017. Ubiquitin modification by the E3 ligase/ADP-ribosyltransferase Dtx3L/Parp9. Mol Cell 66:503–516.e5. https://doi.org/10.1016/j.molcel.2017.04.028.

31. Chan KF, Carolan LA, Druce J, Chappell K, Watterson D, Young P, Korenkov D, Subbarao K, Barr IG, Laurie KL, Reading PC. 2018. Pathogenesis, humoral immune responses, and transmission between cohoused animals in a ferret model of human respiratory syncytial virus infection. J Virol 92:e01322-17. https://doi.org/10.1128/JVI.01322-17.
32. Szarka RJ, Wang N, Gordon L, Nation PN, Smith RH. 1997. A murine model of pulmonary damage induced by lipopolysaccharide via intranasal instillation. J Immunol Methods 202:49–57. https://doi.org/10.1016/s0022-1759(96)00236-0.
33. National Research Council. 2011. Guide for the care and use of laboratory animals, 8th ed. National Academies Press, Washington, DC.
34. Perez-Riverol Y, Bai J, Bandla C, Hewapathirana S, García-Seisdedos D, Kamatchinathan S, Kundu D, Prakash A, Frericks-Zipper A, Eisenacher M, Walzer M, Wang S, Brazma A, Vizcaíno JA. 2022. The PRIDE database resources in 2022: a hub for mass spectrometry-based proteomics evidences. Nucleic Acids Res 50:D543–D552. https://doi.org/10.1093/nar/gkab1038.